Modeling Steel Frame Buildings in Three Dimensions - Part I: Panel Zone and Plastic Hinge Beam Elements

Swaminathan Krishnan [1] and John F. Hall [2]

Keywords: Steel Frames, Nonlinear Analysis, Panel Zone, Plastic Hinge, Earthquake.

ABSTRACT

A procedure for efficient three-dimensional nonlinear time-history analysis of steel framed buildings is derived. It incorporates two types of nonlinear beam elements - the plastic hinge type and the elastofiber type - and nonlinear panel zone elements to model yielding and strain-hardening in moment frames. Floors and roofs of buildings are modeled using 4-node elastic diaphragm elements. The procedure utilizes an iteration strategy applied to an implicit time-integration scheme to solve the nonlinear equations of motion at each time-step. Geometric nonlinearity is included. An overview of the procedure and the theories for the panel zone and the plastic hinge elements are presented in this paper. The theory for the elastofiber element along with illustrative examples are presented in a companion paper. The plastic hinge beam element consists of two nodes at which biaxial flexural yielding is permitted, leading to the formation of plastic hinges. Elastic rotational springs are connected across the plastic hinge locations to model strain-hardening. Axial yielding is also permitted. The panel zone element consists of two orthogonal panels forming a cruciform section. Each panel may yield and strain harden in shear.

[1]Post-Doctoral Scholar, Seismological Laboratory, MC 252-21, California Institute of Technology, Pasadena, CA-91125. Email: krishnan@caltech.edu

[2]Professor, Civil Engineering and Applied Mechanics, MC 104-44, California Institute of Technology, Pasadena, CA-91125

INTRODUCTION

A number of nonlinear analysis programs incorporating various types of beam and column elements have been developed by research groups in seismic engineering. These include OpenSees (Mazzoni, McKenna, and Fenves 2005), ANDERS (Carlson 1999), CU-DYNAMIX (El-Tawil and Deierlein 1996), DRAIN2DX (Allahabadi and Powell 1988), DRAIN3DX (Prakash, Powell, and Campbell 1994; Powell and Campbell 1994), FEDEAS (Filippou and Romero 1998), IDARC (Park, Reinhorn, and Kunnath 1987; Kunnath, Reinhorn, and Lobo 1992; Kunnath 1995), IDARC3D (Lobo 1994), and ISTAR-ST (Lobo, Skokan, Huang, and Hart 1998). A summary of their capabilities is provided by (Carlson 1999).

Of these, the programs that are capable of 3-dimensional modeling are OpenSees, ANDERS, DRAIN3DX, and IDARC3D. OpenSees is a software framework for simulating the seismic response of structural and geotechnical systems. It includes beam-column elements with distributed plasticity integrated along the length of the element. A corotational geometric transformation enables the modeling of large displacements. ANDERS models buildings using planar frames arranged in an orthogonal pattern. Two-dimensional multi-segment fiber elements are employed except for columns at the intersections of the frames where 3-dimensional fiber elements are used to model bi-axial bending behavior. The orthogonal frames are constrained to move together at the floor levels using a master-slave constraint. $P-\Delta$ effects on frame columns in the planes of the frames are automatically accounted for through geometric updating. $P-\Delta$ effects due to out-of-plane displacements are accounted for by applying appropriate force couples on orthogonal frames. DRAIN3DX includes a fully discretized fiber element with a trilinear axial stress-strain law for the fibers. $P-\Delta$ effects are included by adding geometric stiffness to the tangent stiffness matrix for each element and accounting for second order effects in the resisting force computation. IDARC3D is a program developed for the modeling of reinforced concrete structures in which beams and columns are modeled as inelastic single component elements with distributed flexibility. Beam-column elements are modeled using flexural springs with a multi-linear moment-curvature

relationship. Shear deformations are included. Axial deformation is included in the columns but its interaction with bending strength is not. During the time-history analysis, updating of stiffness matrices is carried out only in the event of a stiffness change and a single-step force-equilibrium correction procedure is used. $P-\Delta$ effects are accounted for by a simple equivalent force method.

The computational challenges posed by three-dimensional seismic analysis of tall buildings are addressed here by the development of a comprehensive nonlinear finite element analysis program, FRAME3D (http://www.frame3d.caltech.edu). The focus is on steel moment frames, although braced frames can also be modeled with slight modifications.

There are two distinguishing features of the program. First, a geometric updating feature is provided to accommodate large translations and rotations of the beam elements. This automatically accounts for $P-\Delta$ effects and allows the analysis to follow a building's response well into collapse. Considerable detail is provided here to document the geometric updating capability. Second is the use of computationally efficient elements which incorporate the important types of nonlinear behavior. Full three-dimensional analyses can be made of large, complex structures. At the present time, the element library of FRAME3D includes the following finite elements: (1) 3-dimensional plastic hinge element to model beams and columns, (2) 3-dimensional elastofiber element to model beams and columns, (3) 3-dimensional panel zone element to model the beam-to-column joints in frames and (4) elastic diaphragm element to model the in-plane action of floors and roofs that tie the frames together. The first three element types contain material nonlinearity, and the plastic hinge and elastofiber elements include geometric stiffness.

An overview of the analysis procedure which is the basis for this program is presented in this paper along with the theories for the panel zone element and the plastic hinge element. The theory for the elastofiber element and illustrative examples are given in a companion paper.

DESCRIPTION OF MODEL

The three-dimensional structural model of framed buildings considered here consists of grids of beams and columns. The setup of the model is comprised of three element classes: panel zone elements, beam elements for beams and columns, and diaphragm elements for floors and roofs. The arrangement of these elements in a typical structural model is illustrated in Figure 1. The two beam element types can be used for either beams or columns. Full geometric updating is included in both static and dynamic analyses. This involves updating the locations of the joint nodes, attachment points, and the local beam nodes (shown in Figure 1) as well as the orientations of the local element coordinate systems.

Panel Zone Element

This element models nonlinear shear deformation in the region of the joint where the beams and columns intersect. The joint region consists of a length of column within the depth of the connecting beams. The shear deformation is due primarily to opposing moments from the beams and columns at the joint caused by the frame being subjected to lateral loads (Figure 2). Each panel zone element is associated with a joint node J, K, etc. at the center of the joint where the global degrees of freedom (DOF) are defined. Each panel zone element consists of two orthogonal panels ① and ② which always remain planar and orthogonal. Edges of these panels contain attachment points a, b, c, and d, where beams attach and e and f on the top and bottom where columns attach. The theory of the panel zone element is presented later in this paper.

Beam Element

This element is used to model beams and columns. Two types of beam elements have been developed: plastic hinge type and elastofiber type. The plastic hinge element has 2 nodes with local node numbers 1 and 2, while the elastofiber element consists of 3 segments with 4 nodes. The exte-

rior nodes at the ends of the elastofiber element are numbered 1 and 2, while the interior nodes are numbered 3 and 4. Both types of beam elements consider nonlinear behavior for flexural and axial deformations. Geometric stiffness, i.e., the effect of axial load on flexural stiffness, is included. The theory of the plastic hinge element is presented later in this paper and that of the elastofiber element is presented in the companion paper.

Diaphragm Element

This element is used to model the in-plane stiffness of floor slabs. It is essentially a 4-node plane-stress element connecting to joint nodes J, K, L, and M. Details of the diaphragm element are given by (Krishnan 2003). Its behavior is linearly elastic.

Coordinate Systems

Various coordinate systems are used in the structural model; each set of axes is right-handed and orthogonal. XYZ is the global, fixed coordinate system that is used to define the structure in space. The coordinates of the joint nodes, attachment points, and local beam nodes are with respect to this coordinate system. The Z axis is oriented vertically.

Other coordinate systems are local and are associated with the elements. Separate $\bar{X}\bar{Y}\bar{Z}$ systems are used for each panel zone element, and separate $X'Y'Z'$ systems are used for each plastic hinge element and each segment of each elastofiber element. These local coordinate systems translate and rotate with their associated elements and segments. The orientations of the local axes are defined later, except that it is now noted that $\bar{Y}$ is perpendicular to panel ① of a panel zone element, $\bar{Z}$ is perpendicular to panel ② and $\bar{X}$ is along the panel intersection line $e - f$.

Structure Degrees of Freedom

The global degrees of freedom are associated only with the nodes J, K, etc. at the joints. The structural model consists of 8 global DOF at each node, J. These DOF are listed below. Note that the translational DOF are with respect to the global axes X, Y, Z, and the rotational DOF are with respect to the local sets of panel zone axes, $\bar{X}$, $\bar{Y}$, $\bar{Z}$. The four θ^B and θ^C DOF are shown in Figure 3.

1. U_{JX}: translation in the X direction.
2. U_{JY}: translation in the Y direction.
3. U_{JZ}: translation in the Z direction.
4. $\theta_{J\bar{X}}$: rotation of panel zone element as a rigid body about the $\bar{X}$ axis.
5. $\theta^B_{J\bar{Y}}$: rotation of the line $e-f$ about the $\bar{Y}$ axis. It corresponds to deformation of panel ① into the shape of a parallelogram. The B indicates that the rotating panel edges are connected to beams.
6. $\theta^C_{J\bar{Y}}$: rotation of the line $a-b$ about the $\bar{Y}$ axis. It corresponds to deformation of panel ① into the shape of a parallelogram. The C indicates that the rotating panel edges are connected to columns. Note that $\theta^B_{J\bar{Y}}$ and $\theta^C_{J\bar{Y}}$ together accommodate a rigid rotation of panel ① about $\bar{Y}$ plus its shear deformation.
7. $\theta^B_{J\bar{Z}}$: rotation of the line $e-f$ about the $\bar{Z}$ axis. It corresponds to deformation of panel ② into the shape of a parallelogram. The B indicates that the rotating panel edges are connected to beams.
8. $\theta^C_{J\bar{Z}}$: rotation of the line $c-d$ about the $\bar{Z}$ axis. It corresponds to deformation of panel ② into the shape of a parallelogram. The C indicates that the rotating panel edges are connected to columns. Note that $\theta^B_{J\bar{Z}}$ and $\theta^C_{J\bar{Z}}$ together accommodate a rigid rotation of panel ② about $\bar{Z}$ plus its shear deformation.

Panel zone elements contribute stiffness directly to the four global DOF: $\theta^B_{J\bar{Y}}$, $\theta^C_{J\bar{Y}}$, $\theta^B_{J\bar{Z}}$, and $\theta^C_{J\bar{Z}}$. Beam elements are formulated in terms of 3 translational and 3 rotational DOF at each of the local nodes (1 and 2 for plastic hinge element and 1, 2, 3, and 4 for elastofiber element). However, none of these DOF appear in the global equations. Appropriate stiffness terms from the beam elements are assembled into the global DOF through transformation matrices based on the geometry of the deformed panel zone elements.

Base Condition

Additional modeling considerations, not discussed here in detail, can be employed at the base of the building or at basement levels. Stiffnesses representing foundation flexibility can be assembled into translational DOF in contact with the ground, or those DOF are fixed if the foundation can be assumed to be rigid. Flexible basement walls on the perimeter can be modeled with wall elements, or, again, appropriate DOF are fixed if such walls can be assumed to be rigid. Reference (Hall 1995) contains examples where foundation flexibility and basement walls are considered.

EQUATIONS OF MOTION AND SOLUTION PROCESS

The matrix equation of motion of the building (Cook, Malkus, and Plesha 1989; Chopra 1995) as a function of time, t, is

$$[M]\left\{\ddot{U}(t)\right\} + [C]\left\{\dot{U}(t)\right\} + \{R(t)\} = \{f_g\} - [M]\,[r]\left\{\ddot{U}_g(t)\right\}. \tag{1}$$

In the above,

1. $\{U(t)\}$ = vector of global displacements at time, t, comprising the 8 global translations and rotations at each node, J, K, etc, not including the fixed support DOF.
2. $\left\{\dot{U}(t)\right\}$, $\left\{\ddot{U}(t)\right\}$ = vectors of nodal velocities and accelerations respectively corresponding

to the global translations and rotations at each node.

3. $[M]$ = structure mass matrix. The mass in the structural system is lumped at the joint nodes, rendering the mass matrix diagonal. Further, the rotary inertia of the lumped nodal masses is neglected, so the only non-zero terms of the mass matrix are the diagonal terms corresponding to the translational degrees of freedom.

4. $[C]$ = structure damping matrix. Damping is assumed to be of the Rayleigh type (stiffness and mass proportional). Thus, the damping matrix is computed as,

$$[C] = a_0 [M] + a_1 [K] \tag{2}$$

where a_0 and a_1 are user defined proportionality constants. The initial elastic stiffness matrix is used in the above computation.

5. $\{R(t)\}$ = vector of stiffness forces corresponding to the configuration $\{U(t)\}$. It is computed considering all material and geometric nonlinear effects.

6. $\{f_g\}$ = vector of static gravity loads for which a static analysis is performed first.

7. $\left\{\ddot{U}_g(t)\right\}$ = vector consisting of two horizontal components (X and Y) and one vertical component (Z) of the free-field ground acceleration at time t. The ground motion is assumed spatially uniform.

8. $[r]$ = a 3-column matrix of zeroes except for ones in the first, second, and third columns in the positions corresponding to the X, Y, and Z translational DOF, respectively.

The nonlinear effects contained in $\{R(t)\}$ can be linearized over the time interval between t and $t + \Delta t$ as:

$$\{R(t + \Delta t)\} = [K_T] \{\Delta U\} + \{R(t)\} \tag{3}$$

where $[K_T]$ is the tangent stiffness matrix corresponding to the configuration $\{U(t)\}$. Eqn. 3 is substituted into eqn. 1 written at time $t + \Delta t$ along with the following relations representing a constant average acceleration over the time step Δt:

$$\left\{\dot{U}(t+\Delta t)\right\} = \left\{\dot{U}(t)\right\} + \left\{\ddot{U}(t) + \ddot{U}(t+\Delta t)\right\}\frac{\Delta t}{2} \tag{4a}$$

$$\left\{\ddot{U}(t+\Delta t)\right\} = \frac{4}{(\Delta t)^2}\left\{U(t+\Delta t) - U(t)\right\} - \frac{4}{\Delta t}\left\{\dot{U}(t)\right\} - \left\{\ddot{U}(t)\right\}. \tag{4b}$$

The result is

$$\left[\frac{4}{(\Delta t)^2}M + \frac{2}{\Delta t}C + K_T\right]\{\Delta U\} = \{f_g\} - \{R(t)\} - [M][r]\left\{\ddot{U}_g(t)\right\} + [M]\left\{\frac{4}{\Delta t}\dot{U}(t) + \ddot{U}(t)\right\} + [C]\left\{\dot{U(t)}\right\}. \tag{5}$$

Solution of eqn. 5 for $\{\Delta U\}$ leads to the new displacements via

$$\{U(t+\Delta t)\} = \{U(t)\} + \{\Delta U\}. \tag{6}$$

Once $[K_T]$ and R are updated to time $t + \Delta t$ and $\left\{\dot{U}(t+\Delta t)\right\}$ and $\left\{\ddot{U}(t+\Delta t)\right\}$ are determined from eqns. 4a and 4b, the next time step can commence. This process continues forward in time step by step.

However, since its unlikely that the linearization in eqn. 3 will hold throughout the entire time step without $[K_T]$ changing, iterations are used within each time step. In iteration l, displacement configuration $\left\{U^l\right\}$ has been reached, and the equation to be solved uses $\left[K_T^l\right]$ and $\left\{R^l\right\}$

corresponding to this configuration:

$$\left[\frac{4}{(\Delta t)^2}M + \frac{2}{\Delta t}C + K_T^l\right]\{\Delta U\} = \{f_g\} - \left\{R^l\right\} - [M][r]\left\{\ddot{U}_g(t)\right\} + [M]\left\{\frac{4}{(\Delta t)^2}U(t) + \frac{4}{\Delta t}\dot{U}(t) + \ddot{U}(t)\right\} + [C]\left\{\frac{2}{\Delta t}U(t) + \dot{U}(t)\right\} - \left[\frac{4}{(\Delta t)^2}M + \frac{2}{\Delta t}C\right]\left\{U^l\right\}. \tag{7}$$

Solution of eqn. 7 leads to $\{\Delta U\}$ which adds to $\left\{U^l\right\}$ to give $\left\{U^{l+1}\right\}$. The next iteration uses the updated values of $\left[K_T^{l+1}\right]$ and $\left\{R^{l+1}\right\}$ corresponding to configuration $\left\{U^{l+1}\right\}$. Iterations continue until convergence, and then the next time step begins.

For nonlinear problems, the basic computational task is to update $\left[K_T^l\right]$ and $\left\{R^l\right\}$ using $\{\Delta U\}$. The updating is done at the element level and then assembly is used to construct $\left[K_T^{l+1}\right]$ and $\left\{R^{l+1}\right\}$, i.e., contributions to $\left[K_T^{l+1}\right]$ are the element matrices $\left[K_{pz}^{l+1}\right]$, $\left[K_{ph}^{l+1}\right]$, $\left[K_{ef}^{l+1}\right]$ and $\left[K_d^{l+1}\right]$, and contributions to $\left\{R^{l+1}\right\}$ are the element vectors $\left\{R_{pz}^{l+1}\right\}$, $\left\{R_{ph}^{l+1}\right\}$, $\left\{R_{ef}^{l+1}\right\}$, and $\left\{R_d^{l+1}\right\}$. The subscripts stand for panel zone element, plastic hinge beam element, elastofiber beam element, and diaphragm element, respectively.

Take, for example, computation of the updated $\left[K_{ph}^{l+1}\right]$ and $\left\{R_{ph}^{l+1}\right\}$ for a plastic hinge element. The following steps are performed:

1. The 16 global displacement increments from $\{\Delta U\}$ computed by eqn. 7 for the nodes J and K associated with the plastic hinge element are extracted and placed in the vector $\{\Delta U_{ph}\}$.

2. Using a matrix $\left[T_{ph}^l\right]$, vector $\{\Delta U_{ph}\}$ is transformed into $\left\{\Delta U'_{ph}\right\}_L$ which contains displacement increments for the element's 12 degrees of freedom at nodes 1 and 2 in the $X'Y'Z'$ coordinate system:

$$\left\{\Delta U'_{ph}\right\}_L = \left[T_{ph}^l\right]\{\Delta U_{ph}\}. \tag{8}$$

The subscript L indicates that the vector contains terms for the element's 12 DOF at its local

nodes 1 and 2.

3. The element's displacement increments $\left\{\Delta U'_{ph}\right\}_L$ are used to first compute $\left[K'^{l+1}_{ph}\right]_L$ and $\left\{R'^{l+1}_{ph}\right\}_L$, which are in terms of the element's 12 DOF.

4. Then, $\left[K'^{l+1}_{ph}\right]_L$ and $\left\{R'^{l+1}_{ph}\right\}_L$ are transformed to the 16 global DOF at nodes J and K using the matrix $\left[T^{l+1}_{ph}\right]$ updated to the $l+1$ configuration:

$$\left[K^{l+1}_{ph}\right] = \left[T^{l+1}_{ph}\right]^T \left[K'^{l+1}_{ph}\right]_L \left[T^{l+1}_{ph}\right] \tag{9}$$

$$\left\{R^{l+1}_{ph}\right\} = \left[T^{l+1}_{ph}\right]^T \left\{R'^{l+1}_{ph}\right\}_L . \tag{10}$$

The updating process is a little different for the other element types. Since the θ^B and θ^C degrees of freedom for the panel zone element are also global degrees of freedom, no transformation with a T matrix is necessary. Some additional steps are necessary for the elastofiber element because the presence of interior nodes means that a nonlinear structural analysis problem must be solved for each element, using iterations. These iterations are within those performed during the global solution process. Details for the panel zone and plastic hinge beam elements are provided in the next few sections. Parts dealing with the element tangent stiffness matrices use a differential notation since tangent is a limit concept.

PANEL ZONE ELEMENT

General Description

Each joint is modeled by a panel zone element consisting of a length of column within the depth of the connecting beams. This implies that one column, the associated column of the joint, runs continuously through the height of the joint. The panel zone element is an idealization of the joint region of this column. It consists of two rectangular panels which are perpendicular to each other, panel ① in the $\bar{X}-\bar{Z}$ plane and panel ② in the $\bar{X}-\bar{Y}$ plane, forming a cruciform section (Figures

1 and 4). The thicknesses of all web plates and web doubler plates of the associated column are combined to form the thickness of panel ①, $t_p^{①}$, while the thicknesses of all flange plates of the associated column are combined to form the thickness of panel ②, $t_p^{②}$. The depth D of the joint is taken to be equal to the depth (dimension along the minor axis Z') of the associated column. The width W of the joint is taken to be equal to the width (dimension along the major axis Y'). The height H of the joint is taken to be equal to the depth of the deepest beam framing into that joint. Beams and columns modeled using beam elements connect to the panel zone element at the mid-points of the edges of the two panels. These connection points are referred to as attachment points. There are six attachment points, a through f. Attachment points a, b, c, and d are reserved for beams, while attachment points e and f are reserved for columns.

The panels are assumed to deform only in shear as a result of the end moments and shears of the attached beams and columns. However, they remain planar and perpendicular to each other at all times. The relation between the shear stress τ and the shear strain γ in each panel can be a nonlinear relation. Detailed experimental (Kato 1982; Krawinkler and Popov 1982; Popov and Petersson 1978; Bertero, Popov, and Krawinkler 1972) and analytical (Pinkney 1973; Krawinkler, Bertero, and Popov 1975; Kato 1982; Popov and Petersson 1978; Fielding and Chen 1973) studies have been carried out on steel-frame joints and have resulted in a much better understanding of their hysteretic behavior. A hysteretic model (Hall and Challa 1995) is implemented here as described in the next section.

Each panel has two degrees of freedom as shown in Figure 3: $\theta^B_{J\bar{Y}}$ and $\theta^C_{J\bar{Y}}$ for panel ① and $\theta^B_{J\bar{Z}}$ and $\theta^C_{J\bar{Z}}$ for panel ②, where J is the global node at the center of the joint. These DOF are also global DOF. Strain or rotation in one of the panels causes a rigid body rotation but no strain in the orthogonal panel.

The joint coordinate system $\bar{X}\bar{Y}\bar{Z}$ with origin at the center of the joint (at the node) is defined as follows:

1. $\bar{X}$ axis is oriented from attachment point f to attachment point e of the joint. As the panel

zone element moves and deforms, $\bar{X}$ follows the f-to-e orientation.

2. $\bar{Y}$ axis is in the plane of panel ② and is initially in the d-to-c direction (Figure 4). As the panel zone element moves and deforms, $\bar{Y}$ remains in the plane of panel ② but it may rotate off the d-to-c direction since it must remain perpendicular to $\bar{X}$.

3. $\bar{Z}$ axis is in the plane of panel ① and is initially in the b-to-a direction (Figure 4). As the panel zone element moves and deforms, $\bar{Z}$ remains in the plane of panel ① but it may rotate off the b-to-a direction since it must remain perpendicular to $\bar{X}$.

Material Model for Panel Shear

The hysteresis model for shear stress-strain behavior in a panel proposed by (Hall and Challa 1995) defines a backbone curve as shown in Figure 5. This curve is assumed to be linear until a stress of $0.8\tau_y$ is reached corresponding to a strain of $0.8\gamma_y$, where τ_y and γ_y are the yield shear stress and strain, respectively. The ultimate shear stress τ_u of the panel zone is assumed to be equal to $2.35\tau_y$, with an ultimate shear strain γ_u of $100\gamma_y$. These control points are selected based on monotonic test data on panel zones in beam-column assemblages (Kato 1982). The post-yield behavior is influenced by the resistance of the panel boundary elements (column flanges and continuity plates), and the restraint to deformation of joint-panel by the adjacent beam and column webs, in addition to the strain-hardening of the panel plate. The post-ultimate behavior is assumed to be perfectly plastic. The curve between the joint shear strain limits of $0.8\gamma_y$ and $100\gamma_y$ is defined by a quadratic ellipse. Hysteresis loops are defined by linear segments and cubic ellipses, and the hysteresis rules to define the cyclic response of each panel are given by (Challa 1992). These rules are the same as those used for each fiber in an elastofiber element and are illustrated in Figure 3 of the companion paper.

Theory of the Panel Zone Element

Figure 6 shows panels ① and ② with their dimensions, degrees of freedom, and shear forces acting on the panel edges. The shear forces come from the end moments and shears from the connected beam elements modeling beams and columns. Each panel is under a uniform state of shear stress: $\tau^{①}$ for panel ① and $\tau^{②}$ for panel ②.

Consider panel ① with its degrees of freedom, $\theta^B_{J\bar{Y}}$ and $\theta^C_{J\bar{Y}}$. The four edge forces form a double couple of amplitude $\tau^{①} t_p^{①} HD$. The halves of this double couple are the panel moments which correspond to the two rotational DOF and can be written as

$$M^C_{J\bar{Y}} = -M^B_{J\bar{Y}} = \tau^{①} t_p^{①} HD. \tag{11}$$

The shear stress $\tau^{①}$ is related to the shear strain $\gamma^{①}$ by the incremental relation,

$$d\tau^{①} = G_T^{①} d\gamma^{①} \tag{12}$$

where $G_T^{①}$ is the tangent shear modulus. The incremental shear strain is related to the degrees of freedom by

$$d\gamma^{①} = d\theta^C_{J\bar{Y}} - d\theta^B_{J\bar{Y}}. \tag{13}$$

Combining eqns. 12 and 13 with the incremental version of eqn. 11 leads to

$$\begin{Bmatrix} dM^B_{J\bar{Y}} \\ dM^C_{J\bar{Y}} \end{Bmatrix} = G_T^{①} t_p^{①} HD \begin{bmatrix} 1 & -1 \\ -1 & 1 \end{bmatrix} \begin{Bmatrix} d\theta^B_{J\bar{Y}} \\ d\theta^C_{J\bar{Y}} \end{Bmatrix} \tag{14}$$

which is the tangent relation for panel ①.

A similar treatment for panel ② results in the following tangent relation:

$$\left\{ \begin{array}{c} dM^B_{J\bar{Z}} \\ dM^C_{J\bar{Z}} \end{array} \right\} = G^{②}_T t^{②}_p HW \left[\begin{array}{cc} 1 & -1 \\ -1 & 1 \end{array} \right] \left\{ \begin{array}{c} d\theta^B_{J\bar{Z}} \\ d\theta^C_{J\bar{Z}} \end{array} \right\}. \tag{15}$$

Combining eqns. 14 and 15 leads to

$$\{dR_{pz}\} = [K_{T,pz}]\,\{dU_{pz}\} \tag{16}$$

where $\{dR_{pz}\}$ is the incremental version of

$$\langle R_{pz} \rangle = \langle \; M^B_{J\bar{Y}} \quad M^C_{J\bar{Y}} \quad M^B_{J\bar{Z}} \quad M^C_{J\bar{Z}} \; \rangle, \tag{17}$$

$[K_{T,pz}]$ is the 4x4 tangent stiffness matrix for the panel zone element, and

$$\langle dU_{pz} \rangle = \langle \; d\theta^B_{J\bar{Y}} \quad d\theta^C_{J\bar{Y}} \quad d\theta^B_{J\bar{Z}} \quad d\theta^C_{J\bar{Z}} \; \rangle. \tag{18}$$

Updating Process

In global iteration l, $\{\Delta U\}$ is computed from eqn. 7. The four rotation increments for a panel zone element, $\Delta\theta^B_{J\bar{Y}}$, $\Delta\theta^C_{J\bar{Y}}$, $\Delta\theta^B_{J\bar{Z}}$, and $\Delta\theta^C_{J\bar{Z}}$, are extracted from $\{\Delta U\}$ and placed in $\{\Delta U_{pz}\}$. The coordinates of node J of the panel zone element are updated using ΔU_{JX}, ΔU_{JY}, and ΔU_{JZ}, also obtained from $\{\Delta U\}$. Using the new location of node J and the incremental rotations $\{\Delta U_{pz}\}$ the updated coordinates for attachment points a through f and the updated orientations for the $\bar{X}$, $\bar{Y}$, and $\bar{Z}$ axes are found. The procedure for this geometry updating is given by (Krishnan 2003). Also updated are angles $\xi^{①}$ and $\xi^{②}$ used in the plastic hinge element formulation described later.

Shear strain increments in the two panels are computed as

$$\Delta\gamma^{①} = \Delta\theta^{C}_{J\bar{Y}} - \Delta\theta^{B}_{J\bar{Y}} \tag{19a}$$

$$\Delta\gamma^{②} = \Delta\theta^{B}_{J\bar{Z}} - \Delta\theta^{C}_{J\bar{Z}} \tag{19b}$$

from which the updated shear strains are

$$\gamma^{①,l+1} = \gamma^{①,l} + \Delta\gamma^{①} \tag{20a}$$

$$\gamma^{②,l+1} = \gamma^{②,l} + \Delta\gamma^{②}. \tag{20b}$$

The updated shear stresses $\tau^{①,l+1}$ and $\tau^{②,l+1}$ can now be found using the material model described previously. From eqn. 11, the moments for panel ① are

$$M^{C,l+1}_{J\bar{Y}} = -M^{B,l+1}_{J\bar{Y}} = \tau^{①,l+1} t^{①}_{p} HD. \tag{21}$$

Similarly, the moments for panel ② are given by,

$$M^{C,l+1}_{J\bar{Z}} = -M^{B,l+1}_{J\bar{Z}} = -\tau^{②,l+1} t^{②}_{p} HW. \tag{22}$$

Then, as in eqn. 17,

$$\langle R^{l+1}_{pz} \rangle = \langle \; M^{B,l+1}_{J\bar{Y}} \quad M^{C,l+1}_{J\bar{Y}} \quad M^{B,l+1}_{J\bar{Z}} \quad M^{C,l+1}_{J\bar{Z}} \; \rangle. \tag{23}$$

The element tangent stiffness matrix can be updated once the tangent shear moduli $G^{①,l+1}_{T}$ and $G^{②,l+1}_{T}$ are found for each panel. This information is available as a result of computing $\left\{R^{l+1}_{pz}\right\}$, after which $\left[K^{l+1}_{T,pz}\right]$ can be found from the formulae in the previous section.

Since the rotational DOF of the panel zone element are also global DOF, no transformations of $\left\{R^{l+1}_{pz}\right\}$ and $\left[K^{l+1}_{T,pz}\right]$ are necessary before they are assembled into the global equations.

THREE-DIMENSIONAL PLASTIC HINGE BEAM ELEMENT

General Description

The following assumptions are made in the formulation of this element:

1. The cross-section is uniform along the length of the element.
2. The cross-section is doubly symmetric (with shear center at the centroid).
3. Plane sections remain plane; however, they do not have to remain normal to the beam axis. Thus, shear deformations are included.
4. Strains in the element are small.
5. Lateral deflections relative to the chord are small. This means that the effect of bowing (Oran 1973a; Oran 1973b; Kassimali 1983) on axial stiffness is neglected. This effect is important only for very slender members or during post-buckling of compression members such as braces in braced frames.
6. Warping restraint under twisting is neglected.
7. The element is not loaded along its span.

The plastic hinge beam element has two nodes which connect to the attachment points a through f of the panel zone element. It can model beams and columns in framed structures. Columns connect to attachment points e and f while beams connect to attachment points a through d. The beam element along with its degrees of freedom is shown in Figure 7. Original length of the element is L_0.

The plastic hinge element local coordinate system $X'Y'Z'$ is defined as follows:

1. X' axis runs along the longitudinal axis of the element at the centroid of the cross-section. It is defined as a vector from node 1 to node 2 which are also located at the centroid.

2. Y' axis is orthogonal to X' and is the major principal axis of the cross-section.

3. Z' axis is the minor principal axis of the cross-section.

The major and minor principal axes Y' and Z' of the cross-section are oriented using a user-defined orientation angle α_{or} (Krishnan 2003).

Degrees of Freedom, and Nodal Forces and Moments

The degrees of freedom (Figure 7) of the plastic hinge element are:

1. U_1, U_2 = X' translations of nodes 1 and 2, respectively.

2. $V_{1Y'}$, $V_{2Y'}$ = Y' translations of nodes 1 and 2, respectively.

3. $V_{1Z'}$, $V_{2Z'}$ = Z' translations of nodes 1 and 2, respectively.

4. α_1, α_2 = rotations about X' at nodes 1 and 2, respectively.

5. $\theta_{1Y'}$, $\theta_{2Y'}$ = rotations about Y' at nodes 1 and 2, respectively.

6. $\theta_{1Z'}$, $\theta_{2Z'}$ = rotations about Z' at nodes 1 and 2, respectively.

Corresponding to these DOF are nodal forces and moments (Figure 7):

1. P_1, P_2 = forces in X' direction at nodes 1 and 2, respectively.

2. $Q_{1Y'}$, $Q_{2Y'}$ = forces in Y' direction at nodes 1 and 2, respectively.

3. $Q_{1Z'}$, $Q_{2Z'}$ = forces in Z' direction at nodes 1 and 2, respectively.

4. T_1, T_2 = moments about X' at nodes 1 and 2, respectively.

5. $M_{1Y'}$, $M_{2Y'}$ = moments about Y' at nodes 1 and 2, respectively.

6. $M_{1Z'}$, $M_{2Z'}$ = moments about Z' at nodes 1 and 2, respectively.

Internal Forces and Moments

The internal forces and moments in the plastic hinge beam element are the axial force, P, the shear forces in the Y' and Z' directions, $Q_{Y'}$ and $Q_{Z'}$, respectively, the twisting moment (torque), T, and the bending moments about the Y' and Z' axes, $M_{Y'}$ and $M_{Z'}$, respectively. The sign convention (positive directions) for these forces and moments is shown in Figure 8.

Material Nonlinearity

Two types of material nonlinearity are considered.

1. Axial yielding when axial force P in the element reaches the yield axial force P_y which is given by:

$$P_y = \sigma_y A \tag{24}$$

   where σ_y is the yield stress of the material and A is the area of the cross-section.

2. Flexural yielding when the bending moment $M_{Y'}$ or $M_{Z'}$ at the ends of the element reaches the plastic moment capacity $M_{pY'}$ or $M_{pZ'}$ which depend on the axial force P as shown in Figure 9. The plastic moment capacities when $P = 0$, denoted by $M^0_{pY'}$ and $M^0_{pZ'}$, are given by

$$M^0_{pY'} = \sigma_y Z_{Y'} \tag{25a}$$

$$M^0_{pZ'} = \sigma_y Z_{Z'} \tag{25b}$$

   where $Z_{Y'}$ and $Z_{Z'}$ are the plastic moduli of the cross-section of the element about its major and minor axes, respectively. Once $|M_{Y'}|$ or $|M_{Z'}|$ reaches $M_{pY'}$ or $M_{pZ'}$ at node 1 or node 2, further loading causes a kink, termed a plastic hinge, to form in the beam at that node. Between these plastic hinge locations, the beam behaves elastically. To approximate the

effect of strain hardening, elastic rotational springs are mounted across the plastic hinges to exert moments proportional to the kink angles about the Y' and Z' axes.

Transformation Matrix, $[T_{ph}]$

$[T_{ph}]$ is the transformation matrix between the 16 global DOF at the nodes J and K of the joints, $\{\Delta U_{ph}\}$, and the 12 local degrees of freedom at nodes 1 and 2, $\left\{\Delta U'_{ph}\right\}_L$. For notational purposes, it is assumed that node 1 of the element connects to one of the attachment points at node J and that node 2 of the element connects to one of the attachment points at node K. The transformation is carried out in four steps for displacement increments:

$$\{\Delta U_{ph}\} \xrightarrow{1} \left\{\Delta \bar{U}_{ph}\right\} \xrightarrow{2} \left\{\Delta \bar{U}_{ph}\right\}_L \xrightarrow{3} \{\Delta U_{ph}\}_L \xrightarrow{4} \left\{\Delta U'_{ph}\right\}_L . \tag{26}$$

The global displacement increments in $\{\Delta U_{ph}\}$ are listed as

$$\langle \Delta U_{ph} \rangle = \begin{matrix} \langle \Delta U_{JX} & \Delta U_{JY} & \Delta U_{JZ} & \Delta \theta_{J\bar{X}} & \Delta \theta^B_{J\bar{Y}} & \Delta \theta^C_{J\bar{Y}} & \Delta \theta^B_{J\bar{Z}} & \Delta \theta^C_{J\bar{Z}} \\ \Delta U_{KX} & \Delta U_{KY} & \Delta U_{KZ} & \Delta \theta_{K\bar{X}} & \Delta \theta^B_{K\bar{Y}} & \Delta \theta^C_{K\bar{Y}} & \Delta \theta^B_{K\bar{Z}} & \Delta \theta^C_{K\bar{Z}} \rangle \end{matrix} . \tag{27}$$

In $\{\Delta U_{ph}\}$, translational DOF are with respect to XYZ; rotational DOF are with respect to the respective $\bar{X}\bar{Y}\bar{Z}$'s at the nodes J and K.

The first transformation

$$\left\{\Delta \bar{U}_{ph}\right\} = [T_1] \{\Delta U_{ph}\} \tag{28a}$$

produces

$$\langle \Delta \bar{U}_{ph} \rangle = \begin{matrix} \langle \Delta U_{J\bar{X}} & \Delta U_{J\bar{Y}} & \Delta U_{J\bar{Z}} & \Delta \theta_{J\bar{X}} & \Delta \theta^B_{J\bar{Y}} & \Delta \theta^C_{J\bar{Y}} & \Delta \theta^B_{J\bar{Z}} & \Delta \theta^C_{J\bar{Z}} \\ \Delta U_{K\bar{X}} & \Delta U_{K\bar{Y}} & \Delta U_{K\bar{Z}} & \Delta \theta_{K\bar{X}} & \Delta \theta^B_{K\bar{Y}} & \Delta \theta^C_{K\bar{Y}} & \Delta \theta^B_{K\bar{Z}} & \Delta \theta^C_{K\bar{Z}} \rangle \end{matrix} \tag{28b}$$

where the translational DOF are also now with respect to the $\bar{X}\bar{Y}\bar{Z}$'s at nodes J and K.

The second transformation

$$\left\{\Delta\bar{U}_{ph}\right\}_L = [T_2]\left\{\Delta\bar{U}_{ph}\right\} \tag{29a}$$

produces

$$\langle\Delta\bar{U}_{ph}\rangle_L = \langle\Delta U_{1\bar{X}} \quad \Delta U_{1\bar{Y}} \quad \Delta U_{1\bar{Z}} \quad \Delta\theta_{1\bar{X}} \quad \Delta\theta_{1\bar{Y}} \quad \Delta\theta_{1\bar{Z}} \quad \Delta U_{2\bar{X}} \quad \Delta U_{2\bar{Y}} \quad \Delta U_{2\bar{Z}} \quad \Delta\theta_{2\bar{X}} \quad \Delta\theta_{2\bar{Y}} \quad \Delta\theta_{2\bar{Z}}\rangle \tag{29b}$$

where the 8 DOF at node J have been transformed to the 6 local beam DOF at node 1 (still in node J's $\bar{X}\bar{Y}\bar{Z}$) and the 8 DOF at node K have been transformed to the 6 local beam DOF at node 2 (still in node K's $\bar{X}\bar{Y}\bar{Z}$). The subscript L denotes the presence of the terms for the 12 DOF at local nodes 1 and 2.

The third transformation

$$\left\{\Delta U_{ph}\right\}_L = [T_3]\left\{\Delta\bar{U}_{ph}\right\}_L \tag{30a}$$

produces

$$\langle\Delta U_{ph}\rangle_L = \langle\Delta U_{1X} \quad \Delta U_{1Y} \quad \Delta U_{1Z} \quad \Delta\theta_{1X} \quad \Delta\theta_{1Y} \quad \Delta\theta_{1Z} \quad \Delta U_{2X} \quad \Delta U_{2Y} \quad \Delta U_{2Z} \quad \Delta\theta_{2X} \quad \Delta\theta_{2Y} \quad \Delta\theta_{2Z}\rangle \tag{30b}$$

where all DOF are now in XYZ.

Finally, the fourth transformation

$$\left\{\Delta U'_{ph}\right\}_L = [T_4]\left\{\Delta U_{ph}\right\}_L \tag{31a}$$

produces

$$\langle\Delta U'_{ph}\rangle_L = \langle\Delta U_1 \quad \Delta V_{1Y'} \quad \Delta V_{1Z'} \quad \Delta\alpha_1 \quad \Delta\theta_{1Y'} \quad \Delta\theta_{1Z'} \quad \Delta U_2 \quad \Delta V_{2Y'} \quad \Delta V_{2Z'} \quad \Delta\alpha_2 \quad \Delta\theta_{2Y'} \quad \Delta\theta_{2Z'}\rangle \tag{31b}$$

where all DOF are now in the beam element's local $X'Y'Z'$.

Combining the above leads to

$$\left\{\Delta U'_{ph}\right\}_L = [T_{ph}]\left\{\Delta U_{ph}\right\} \tag{32a}$$

where

$$[T_{ph}] = [T_4]\,[T_3]\,[T_2]\,[T_1]\,. \tag{32b}$$

The components, $[T_1]$, $[T_3]$, and $[T_4]$ are defined below.

$$[T_1]^{(16\times16)} = \begin{bmatrix} \left[\bar{C}_J\right]^{(3\times3)} & [0]^{(3\times5)} & [0]^{(3\times3)} & [0]^{(3\times5)} \\ [0]^{(5\times3)} & [I]^{(5\times5)} & [0]^{(5\times3)} & [0]^{(5\times5)} \\ [0]^{(3\times3)} & [0]^{(3\times5)} & \left[\bar{C}_K\right]^{(3\times3)} & [0]^{(3\times5)} \\ [0]^{(5\times3)} & [0]^{(5\times5)} & [0]^{(5\times3)} & [I]^{(5\times5)} \end{bmatrix} \tag{33}$$

where $[I]$ is the 5×5 identity matrix and $\left[\bar{C}_J\right]$ is a matrix consisting of the direction cosines of the panel zone coordinate system $\bar{X}\bar{Y}\bar{Z}$ at joint node J with respect to the global coordinate system XYZ, similar for $\left[\bar{C}_K\right]$ at joint node K.

$$[T_3]^{(12\times12)} = \begin{bmatrix} \left[\bar{C}_J\right]^{T(3\times3)} & [0]^{(3\times3)} & [0]^{(3\times3)} & [0]^{(3\times3)} \\ [0]^{(3\times3)} & \left[\bar{C}_J\right]^{T(3\times3)} & [0]^{(3\times3)} & [0]^{(3\times3)} \\ [0]^{(3\times3)} & [0]^{(3\times3)} & \left[\bar{C}_K\right]^{T(3\times3)} & [0]^{(3\times3)} \\ [0]^{(3\times3)} & [0]^{(3\times3)} & [0]^{(3\times3)} & \left[\bar{C}_K\right]^{T(3\times3)} \end{bmatrix} \tag{34}$$

$$[T_4]^{(12\times12)} = \begin{bmatrix} [C']^{(3\times3)} & [0]^{(3\times3)} & [0]^{(3\times3)} & [0]^{(3\times3)} \\ [0]^{(3\times3)} & [C']^{(3\times3)} & [0]^{(3\times3)} & [0]^{(3\times3)} \\ [0]^{(3\times3)} & [0]^{(3\times3)} & [C']^{(3\times3)} & [0]^{(3\times3)} \\ [0]^{(3\times3)} & [0]^{(3\times3)} & [0]^{(3\times3)} & [C']^{(3\times3)} \end{bmatrix} \tag{35}$$

where $[C']$ is a matrix consisting of the direction cosines of the beam local coordinate system $X'Y'Z'$ with respect to the global coordinate system XYZ.

$[T_2]$ is different for beams and columns. It also depends on the attachment points to which the element local nodes 1 and 2 are connected at nodes J and K. As an example, the following matrix is derived for a column whose local node 1 connects to attachment point f at node J and local node 2 connects to attachment point e at node K. The deformed panel zone geometry which is the source of some of the terms of $[T_2]$ for a column is shown in Figure 10. For instance, an incremental twist in the joint (about the joint $\bar{X}$ axis) leads to an equal amount of incremental twist in the columns that the joint is part of. Hence term [4,4] of the $[T_2]$ matrix in eqn. 36 is 1.0.

$$[T]_2^{col-f-e(12\times16)} = \left[\begin{array}{cccccccc|cccccccc}
1.0 & 0.0 & 0.0 & 0.0 & 0.0 & 0.0 & 0.0 & 0.0 & 0.0 & 0.0 & 0.0 & 0.0 & 0.0 & 0.0 & 0.0 & 0.0 \\
0.0 & 1.0 & 0.0 & 0.0 & 0.0 & 0.0 & -0.5H_J & 0.0 & 0.0 & 0.0 & 0.0 & 0.0 & 0.0 & 0.0 & 0.0 & 0.0 \\
0.0 & 0.0 & 1.0 & 0.0 & 0.5H_J & 0.0 & 0.0 & 0.0 & 0.0 & 0.0 & 0.0 & 0.0 & 0.0 & 0.0 & 0.0 & 0.0 \\
0.0 & 0.0 & 0.0 & 1.0 & 0.0 & 0.0 & 0.0 & 0.0 & 0.0 & 0.0 & 0.0 & 0.0 & 0.0 & 0.0 & 0.0 & 0.0 \\
0.0 & 0.0 & 0.0 & 0.0 & 0.0 & 1.0 & 0.0 & 0.0 & 0.0 & 0.0 & 0.0 & 0.0 & 0.0 & 0.0 & 0.0 & 0.0 \\
0.0 & 0.0 & 0.0 & 0.0 & 0.0 & 0.0 & 0.0 & 1.0 & 0.0 & 0.0 & 0.0 & 0.0 & 0.0 & 0.0 & 0.0 & 0.0 \\
\hline
0.0 & 0.0 & 0.0 & 0.0 & 0.0 & 0.0 & 0.0 & 0.0 & 1.0 & 0.0 & 0.0 & 0.0 & 0.0 & 0.0 & 0.0 & 0.0 \\
0.0 & 0.0 & 0.0 & 0.0 & 0.0 & 0.0 & 0.0 & 0.0 & 0.0 & 1.0 & 0.0 & 0.0 & 0.0 & 0.0 & 0.5H_K & 0.0 \\
0.0 & 0.0 & 0.0 & 0.0 & 0.0 & 0.0 & 0.0 & 0.0 & 0.0 & 0.0 & 1.0 & 0.0 & -0.5H_K & 0.0 & 0.0 & 0.0 \\
0.0 & 0.0 & 0.0 & 0.0 & 0.0 & 0.0 & 0.0 & 0.0 & 0.0 & 0.0 & 0.0 & 1.0 & 0.0 & 0.0 & 0.0 & 0.0 \\
0.0 & 0.0 & 0.0 & 0.0 & 0.0 & 0.0 & 0.0 & 0.0 & 0.0 & 0.0 & 0.0 & 0.0 & 0.0 & 1.0 & 0.0 & 0.0 \\
0.0 & 0.0 & 0.0 & 0.0 & 0.0 & 0.0 & 0.0 & 0.0 & 0.0 & 0.0 & 0.0 & 0.0 & 0.0 & 0.0 & 0.0 & 1.0
\end{array}\right] \tag{36}$$

The deformed panel zone geometry for calculating some of the terms of $[T_2]$ for a beam is shown in Figures 11 and 12. As another example, the following matrix is derived for a beam whose local node 1 connects to attachment point a at node J and local node 2 connects to attachment point b at node K. For instance, an incremental twist in the joint leads to a translation of all the beam attachment points of the joint (as shown in Figure 12). Hence term [2,4] of the $[T_2]$ matrix in eqn. 37 is $-0.5D_J \cos\xi_J^{①}$.

$$[T]_2^{bm-a-b(12\times 16)} =$$

$$\left[\begin{array}{cccccccc|cccccccc}
1.0 & 0.0 & 0.0 & 0.0 & 0.0 & 0.5D_J\cos\xi_J^{①} & 0.0 & 0.0 & 0.0 & 0.0 & 0.0 & 0.0 & 0.0 & 0.0 & 0.0 & 0.0 \\
0.0 & 1.0 & 0.0 & -0.5D_J\cos\xi_J^{①} & 0.0 & 0.0 & 0.0 & 0.0 & 0.0 & 0.0 & 0.0 & 0.0 & 0.0 & 0.0 & 0.0 & 0.0 \\
0.0 & 0.0 & 1.0 & 0.0 & 0.0 & -0.5D_J\sin\xi_J^{①} & 0.0 & 0.0 & 0.0 & 0.0 & 0.0 & 0.0 & 0.0 & 0.0 & 0.0 & 0.0 \\
0.0 & 0.0 & 0.0 & 1.0 & 0.0 & 0.0 & 0.0 & 0.0 & 0.0 & 0.0 & 0.0 & 0.0 & 0.0 & 0.0 & 0.0 & 0.0 \\
0.0 & 0.0 & 0.0 & 0.0 & 1.0 & 0.0 & 0.0 & 0.0 & 0.0 & 0.0 & 0.0 & 0.0 & 0.0 & 0.0 & 0.0 & 0.0 \\
0.0 & 0.0 & 0.0 & 0.0 & 0.0 & 0.0 & 0.5 & 0.5 & 0.0 & 0.0 & 0.0 & 0.0 & 0.0 & 0.0 & 0.0 & 0.0 \\
\hline
0.0 & 0.0 & 0.0 & 0.0 & 0.0 & 0.0 & 0.0 & 0.0 & 1.0 & 0.0 & 0.0 & 0.0 & 0.0 & -0.5D_K\cos\xi_K^{①} & 0.0 & 0.0 \\
0.0 & 0.0 & 0.0 & 0.0 & 0.0 & 0.0 & 0.0 & 0.0 & 0.0 & 1.0 & 0.0 & 0.5D_K\cos\xi_K^{①} & 0.0 & 0.0 & 0.0 & 0.0 \\
0.0 & 0.0 & 0.0 & 0.0 & 0.0 & 0.0 & 0.0 & 0.0 & 0.0 & 0.0 & 1.0 & 0.0 & 0.0 & 0.5D_K\sin\xi_K^{①} & 0.0 & 0.0 \\
0.0 & 0.0 & 0.0 & 0.0 & 0.0 & 0.0 & 0.0 & 0.0 & 0.0 & 0.0 & 0.0 & 1.0 & 0.0 & 0.0 & 0.0 & 0.0 \\
0.0 & 0.0 & 0.0 & 0.0 & 0.0 & 0.0 & 0.0 & 0.0 & 0.0 & 0.0 & 0.0 & 0.0 & 1.0 & 0.0 & 0.0 & 0.0 \\
0.0 & 0.0 & 0.0 & 0.0 & 0.0 & 0.0 & 0.0 & 0.0 & 0.0 & 0.0 & 0.0 & 0.0 & 0.0 & 0.0 & 0.5 & 0.5
\end{array}\right] \tag{37}$$

The angles $\xi^{①}$ and $\xi^{②}$, the latter needed for a beam which connects to attachment points c and d, are defined in Figure 11. The details of how the $[T_2]$ matrix is computed in other instances are given in (Krishnan 2003)

Development of the Tangent Stiffness Matrix

Axial Deformation

The axial force P in the element is a function of the axial strain ϵ as shown in Figure 13. ϵ is the axial strain at the centroid of the cross-section. Increments in P and ϵ are related by

$$dP = E_T A d\epsilon \tag{38a}$$

where E_T is the tangent modulus, either Young's modulus E or zero as shown in Figure 13, and A is the area of the cross-section. The tangent stiffness relation for the nodal forces P_1 and P_2

associated with axial deformation is given by

$$\left\{ \begin{array}{c} dP_1 \\ dP_2 \end{array} \right\} = \frac{E_T A}{L_0} \left[\begin{array}{cc} 1 & -1 \\ -1 & 1 \end{array} \right] \left\{ \begin{array}{c} dU_1 \\ dU_2 \end{array} \right\}. \tag{38b}$$

Twisting

Twisting is assumed to be linearly elastic with increments in torque T and twisting strain ω (twist per unit length) related by

$$dT = GJd\omega \tag{39a}$$

where G is the shear modulus and J is the torsional constant of the cross-section. The tangent stiffness relation for the nodal forces T_1 and T_2 associated with twisting deformation is given by

$$\left\{ \begin{array}{c} dT_1 \\ dT_2 \end{array} \right\} = \frac{GJ}{L_0} \left[\begin{array}{cc} 1 & -1 \\ -1 & 1 \end{array} \right] \left\{ \begin{array}{c} d\alpha_1 \\ d\alpha_2 \end{array} \right\}. \tag{39b}$$

Bending and Shearing in the $X'-Z'$ Plane (Bending about the Major Axis of the Cross-Section)

Figure 14 shows the plastic hinge beam element with the plastic hinges located along the beam just inside the nodes ("inside" means the side towards the middle of the beam). $\phi_{1Y'}$ and $\phi_{2Y'}$ are the Y' rotations of the cross-section between the plastic hinges and the nodes, and $\hat{\phi}_{1Y'}$ and $\hat{\phi}_{2Y'}$ are the Y' rotations of the cross-section just inside the plastic hinges. These rotations are relative to the chord (straight line connecting nodes 1 and 2). Since the behavior between the plastic hinges is elastic,

$$\left\{ \begin{array}{c} M_{1Y'} \\ M_{2Y'} \end{array} \right\} = \left[\begin{array}{cc} a & b \\ b & c \end{array} \right] \left\{ \begin{array}{c} \hat{\phi}_{1Y'} \\ \hat{\phi}_{2Y'} \end{array} \right\} \tag{40}$$

where a, b, and c depend on E, the moment of inertia $I_{Y'}$ about the major axis, G (since shear deformations will be included (Przemeniecki 1968)), the effective shear area $A_{SZ'}$ as shown in Figure 15, and P (since effect of axial load on stiffness will be included (Salmon and Johnson 1980)). For convenience, subscripts denoting the $X' - Z'$ plane will be omitted on a, b, and c.

Solutions for a, b, and c (Hall and Challa 1995) come from the following differential equations:

$$\frac{d^2 M_{Y'}}{dX'^2} + Q_{Z'} = P\frac{d^2 V_{Z'}}{dX'^2} \tag{41a}$$

$$\frac{dQ_{Z'}}{dX'} = 0 \tag{41b}$$

$$M_{Y'} = -EI_{Y'}\frac{d\hat{\phi}_{Y'}}{dX'} \tag{41c}$$

$$Q_{Z'} = GA_{SZ'}\left(\frac{dV_{Z'}}{dX'} + \hat{\phi}_{Y'}\right) \tag{41d}$$

subject to $V_{Z'} = 0$ at nodes 1 and 2, and $\hat{\phi}_{Y'} = \hat{\phi}_{1Y'}$ at node 1, and $\hat{\phi}_{Y'} = \hat{\phi}_{2Y'}$ at node 2. In these equations, $V_{Z'}$ is the Z' translation along the beam relative to the chord, and $\hat{\phi}_{Y'}$ is the Y' rotation of the cross-section along the beam relative to the chord.

Each moment $M_{1Y'}$ and $M_{2Y'}$ consists of a part carried by the plastic hinge and a part carried by the rotational spring:

$$M_{1Y'} = M^h_{1Y'} + M^s_{1Y'} \tag{42a}$$

$$M_{2Y'} = M^h_{2Y'} + M^s_{2Y'}. \tag{42b}$$

The hinge contribution is a rigid-plastic function of the kink rotation as shown in Figure 16 and the spring contribution is a linear function of the kink rotation:

$$M^s_{1Y'} = k_1\kappa_{1Y'} \tag{43a}$$

$$M^s_{2Y'} = k_2\kappa_{2Y'} \tag{43b}$$

where the rotational spring constants at the two ends of the element are k_1 and k_2 (subscripts to indicate the $X' - Z'$ plane are omitted for convenience), and $\kappa_{1Y'}$ and $\kappa_{2Y'}$ are the kink angles given by

$$\kappa_{1Y'} = \phi_{1Y'} - \hat{\phi}_{1Y'} \tag{44a}$$

$$\kappa_{2Y'} = \phi_{2Y'} - \hat{\phi}_{2Y'} \tag{44b}$$

as shown in Figure 14. Substituting eqns. 44 into eqn. 40:

$$\begin{Bmatrix} M_{1Y'} \\ M_{2Y'} \end{Bmatrix} = \begin{bmatrix} a & b \\ b & c \end{bmatrix} \begin{Bmatrix} \phi_{1Y'} - \kappa_{1Y'} \\ \phi_{2Y'} - \kappa_{2Y'} \end{Bmatrix} \tag{45}$$

Taking the differential form, dropping terms containing dP, and with appropriate substitutions from above, this equation can be rewritten as

$$\begin{Bmatrix} dM_{1Y'} \\ dM_{2Y'} \end{Bmatrix} = \begin{bmatrix} a_T & b_T \\ b_T & c_T \end{bmatrix} \begin{Bmatrix} d\phi_{1Y'} \\ d\phi_{2Y'} \end{Bmatrix} \tag{46}$$

where a_T, b_T, and c_T are tangent stiffness coefficients which depend on whether plastic hinges are active during the increment (Table 1).

Equation 46 needs to be transformed and expanded to the nodal degrees of freedom. The

following equations are employed:

$$\begin{Bmatrix} d\phi_{1Y'} \\ d\phi_{2Y'} \end{Bmatrix} = [S] \begin{Bmatrix} dV_{1Z'} \\ d\theta_{1Y'} \\ dV_{2Z'} \\ d\theta_{2Y'} \end{Bmatrix} \tag{47a}$$

$$\begin{Bmatrix} dQ_{1Z'} \\ dM_{1Y'} \\ dQ_{2Z'} \\ dM_{2Y'} \end{Bmatrix} = [S]^T \begin{Bmatrix} dM_{1Y'} \\ dM_{2Y'} \end{Bmatrix} + \frac{P}{L_0} \begin{bmatrix} 1 & 0 & -1 & 0 \\ 0 & 0 & 0 & 0 \\ -1 & 0 & 1 & 0 \\ 0 & 0 & 0 & 0 \end{bmatrix} \begin{Bmatrix} dV_{1Z'} \\ d\theta_{1Y'} \\ dV_{2Z'} \\ d\theta_{2Y'} \end{Bmatrix} \tag{47b}$$

where,

$$[S] = \begin{bmatrix} -\frac{1}{L_0} & 1 & \frac{1}{L_0} & 0 \\ -\frac{1}{L_0} & 0 & \frac{1}{L_0} & 1 \end{bmatrix}$$

and the $\frac{P}{L_0}$ term is additional geometric stiffness.

Combining with eqn. 46 leads to

$$\begin{Bmatrix} dQ_{1Z'} \\ dM_{1Y'} \\ dQ_{2Z'} \\ dM_{2Y'} \end{Bmatrix} = \left[[S]^T \begin{bmatrix} a_T & b_T \\ b_T & c_T \end{bmatrix} [S] + \frac{P}{L_0} \begin{bmatrix} 1 & 0 & -1 & 0 \\ 0 & 0 & 0 & 0 \\ -1 & 0 & 1 & 0 \\ 0 & 0 & 0 & 0 \end{bmatrix} \right] \begin{Bmatrix} dV_{1Z'} \\ d\theta_{1Y'} \\ dV_{2Z'} \\ d\theta_{2Y'} \end{Bmatrix} \tag{48}$$

which is the tangent stiffness relation for the nodal quantities associated with bending and shearing in the $X' - Z'$ plane.

Bending and Shearing in the $X'-Y'$ Plane (Bending about the Minor Axis of the Cross-Section)

A formulation similar to the preceding section leads to

$$\begin{Bmatrix} dQ_{1Y'} \\ dM_{1Z'} \\ dQ_{2Y'} \\ dM_{2Z'} \end{Bmatrix} = \left[[S]^T \begin{bmatrix} a_T & b_T \\ b_T & c_T \end{bmatrix} [S] + \frac{P}{L_0} \begin{bmatrix} 1 & 0 & -1 & 0 \\ 0 & 0 & 0 & 0 \\ -1 & 0 & 1 & 0 \\ 0 & 0 & 0 & 0 \end{bmatrix} \right] \begin{Bmatrix} dV_{1Y'} \\ d\theta_{1Z'} \\ dV_{2Y'} \\ d\theta_{2Z'} \end{Bmatrix} \tag{49}$$

where,

$$[S] = \begin{bmatrix} \frac{1}{L_0} & 1 & -\frac{1}{L_0} & 0 \\ \frac{1}{L_0} & 0 & -\frac{1}{L_0} & 1 \end{bmatrix}$$

and a_T, b_T, and c_T in terms of a, b, and c are as described previously except that a, b, and c use the minor axis moment of inertia $I_{Z'}$ and the effective shear area $A_{SY'}$ (Figure 15).

Combined Results

The tangent relations in eqns. 38b, 39b, 48, and 49 are combined into

$$\left\{dR'_{ph}\right\}_L = \left[K'_{T,ph}\right]_L \left\{dU'_{ph}\right\}_L \tag{50}$$

where L refers to local nodes 1 and 2, $\left\{dR'_{ph}\right\}_L$ is the incremental version of

$$\langle R'_{ph} \rangle_L = \langle \; P_1 \quad Q_{1Y'} \quad Q_{1Z'} \quad T_1 \quad M_{1Y'} \quad M_{1Z'} \quad P_2 \quad Q_{2Y'} \quad Q_{2Z'} \quad T_2 \quad M_{2Y'} \quad M_{2Z'} \; \rangle, \tag{51a}$$

$\left[K'_{T,ph}\right]_L$ is the 12×12 tangent stiffness matrix for the plastic hinge element, and

$$\langle dU'_{ph} \rangle_L = \langle \; dU_1 \quad dV_{1Y'} \quad dV_{1Z'} \quad d\alpha_1 \quad d\theta_{1Y'} \quad d\theta_{1Z'} \quad dU_2 \quad dV_{2Y'} \quad dV_{2Z'} \quad d\alpha_2 \quad d\theta_{2Y'} \quad d\theta_{2Z'} \; \rangle. \tag{51b}$$

Updating Process

In global iteration l, $\{\Delta U\}$ is computed from eqn. 7. The 12 displacement increments in $X'Y'Z'$ at nodes 1 and 2 for a plastic hinge element are found as

$$\left\{\Delta U'_{ph}\right\}_L = \left[T^l_{ph}\right] \{\Delta U_{ph}\} \tag{52}$$

where $\{\Delta U_{ph}\}$ contains the 16 terms extracted from $\{\Delta U\}$ corresponding to joint nodes J and K connected to element nodes 1 and 2, and $\left[T^l_{ph}\right]$ is the transformation matrix representing configuration l.

Updating the panel zone element geometries as discussed previously will produce new locations for the attachment points, from which new $\bar{X}$, $\bar{Y}$, and $\bar{Z}$ orientations can be found, leading to $\left[\bar{C}^{l+1}_J\right]$ and $\left[\bar{C}^{l+1}_K\right]$ and then $\left[T^{l+1}_1\right]$ and $\left[T^{l+1}_3\right]$ by eqns. 33 and 34 respectively. Updating $\xi^{①}$ and $\xi^{②}$ leads to $\left[T^{l+1}_2\right]$ for a beam (eqn. 37 for example); $\left[T^{l+1}_2\right]$ for a column does not need updating (eqn. 36 for example). The new attachment point locations also give the new locations for nodes 1 and 2, and these will give the updated direction for the X' axis of the plastic hinge element. Next, the updated value for α_{or} is found as

$$\alpha^{l+1}_{or} = \alpha^l_{or} + \frac{\Delta\alpha_1 + \Delta\alpha_2}{2} \tag{53}$$

from which the new directions for Y' and Z' are found. The updated direction cosine matrix

$\left[C'^{l+1}\right]$ is then used to form $\left[T_4^{l+1}\right]$ by eqn. 35. Then,

$$\left[T_{ph}^{l+1}\right] = \left[T_4^{l+1}\right]\left[T_3^{l+1}\right]\left[T_2^{l+1}\right]\left[T_1^{l+1}\right]. \tag{54}$$

Next $\left\{R_{ph}'^{l+1}\right\}_L$ is found from $\left\{R_{ph}'^{l}\right\}_L$ and $\left\{\Delta U_{ph}'\right\}_L$. Consider first the nodal axial forces P_1^{l+1} and P_2^{l+1}. Once the locations for nodes 1 and 2 are determined, the new element length L^{l+1} can be found. Then

$$\epsilon^{l+1} = \frac{L^{l+1} - L_0}{L_0} \tag{55a}$$

$$\text{and} \quad \Delta\epsilon = \epsilon^{l+1} - \epsilon^{l}. \tag{55b}$$

Using ϵ^l and $\Delta\epsilon$, P^{l+1} can be found from Figure 13. Then,

$$P_1^{l+1} = -P_2^{l+1} = P^{l+1}. \tag{55c}$$

Next consider the nodal torques T_1^{l+1} and T_2^{l+1}. The increment in twisting strain is

$$\Delta\omega = \frac{\Delta\alpha_2 - \Delta\alpha_1}{L_0} \tag{56a}$$

and then

$$T^{l+1} = T^l + GJ\Delta\omega. \tag{56b}$$

Nodal values are

$$T_1^{l+1} = -T_2^{l+1} = T^{l+1}. \tag{56c}$$

Next is the $X' - Z'$ plane bending and shearing. The $l+1$ state will correspond to one of nine

plastic hinge cases which are listed in Table 2. The procedure is as follows. The nodal ϕ rotations are first updated as

$$\phi_{1Y'}^{l+1} = \phi_{1Y'}^{l} + \Delta\theta_{1Y'} + \frac{\Delta V_{2Z'} - \Delta V_{1Z'}}{L_0} \tag{57a}$$

$$\phi_{2Y'}^{l+1} = \phi_{2Y'}^{l} + \Delta\theta_{2Y'} + \frac{\Delta V_{2Z'} - \Delta V_{1Z'}}{L_0} \tag{57b}$$

Second, the plastic moment capacity is updated to $M_{pY'}^{l+1}$ according to Figure 9 using P^{l+1}. Then each case is examined using eqn. 45 written for state $l+1$:

$$\left\{ \begin{array}{c} M_{1Y'}^{l+1} \\ M_{2Y'}^{l+1} \end{array} \right\} = \left[\begin{array}{cc} a^{l+1} & b^{l+1} \\ b^{l+1} & c^{l+1} \end{array} \right] \left\{ \begin{array}{c} \phi_{1Y'}^{l+1} - \kappa_{1Y'}^{l+1} \\ \phi_{2Y'}^{l+1} - \kappa_{2Y'}^{l+1} \end{array} \right\} \tag{58}$$

where a^{l+1}, b^{l+1}, and c^{l+1} are computed using P^{l+1}.

To examine Case 1, $\kappa_{1Y'}^{l+1} = \kappa_{1Y'}^{l}$ and $\kappa_{2Y'}^{l+1} = \kappa_{2Y'}^{l}$ are substituted into eqn. 58, and $M_{1Y'}^{l+1}$ and $M_{2Y'}^{l+1}$ are computed. Then, if $\left|M_{1Y'}^{l+1}\right| < M_{pY'}^{l+1}$ and $\left|M_{2Y'}^{l+1}\right| < M_{pY'}^{l+1}$, the current state corresponds to Case 1 and the updated moments are accepted.

If Case 1 does not check, Case 2 is examined. $M_{1Y'}^{l+1} = M_{pY'}^{l+1}$ and $\kappa_{2Y'}^{l+1} = \kappa_{2Y'}^{l}$ are substituted into eqn. 58, and the set of eqns. is solved for $M_{2Y'}^{l+1}$ and $\kappa_{1Y'}^{l+1}$. If $\left|M_{2Y'}^{l+1}\right| < M_{pY'}^{l+1}$ and $\kappa_{1Y'}^{l+1} > \kappa_{1Y'}^{l}$, the current state corresponds to Case 2 and the updated moments are accepted. If not, Case 3 is examined and so on. Only one out of the nine cases will check. Finally,

$$-Q_{1Z'}^{l+1} = Q_{2Z'}^{l+1} = \frac{M_{1Y'}^{l+1} + M_{2Y'}^{l+1}}{L^{l+1}}. \tag{59}$$

For $X' - Y'$ plane bending, $Q_{1Y'}^{l+1}$, $M_{1Z'}^{l+1}$, $Q_{2Y'}^{l+1}$, and $M_{2Z'}^{l+1}$ are found by a procedure similar to the one just described. Then the 12 updated nodal forces and moments are assembled into $\left\{R_{ph}^{\prime l+1}\right\}_L$.

The element tangent stiffness matrix can be updated once the updated axial force P^{l+1} and

the appropriate plastic hinge cases for the $X' - Z'$ and $X' - Y'$ planes are determined. This information is available as a result of computing $\left\{R'^{l+1}_{ph}\right\}_L$, after which $\left[K'^{l+1}_{T,ph}\right]_L$ can be found from the formulae in the preceding section.

The final step is the transformation to the global DOF:

$$\left[K^{l+1}_{T,ph}\right] = \left[T^{l+1}_{ph}\right]^T \left[K'^{l+1}_{T,ph}\right]_L \left[T^{l+1}_{ph}\right] \tag{60a}$$

$$\left\{R^{l+1}_{ph}\right\} = \left[T^{l+1}_{ph}\right]^T \left\{R'^{l+1}_{ph}\right\}_L \tag{60b}$$

and then assembly into $\left[K^{l+1}_T\right]$ and $\left\{R^{l+1}\right\}$.

Use of Interior Nodes

A multi-segment plastic hinge element with interior nodes can extend the formulation of the 2-node element just described. Static gravity loads can be applied to the interior nodes, relieving the assumption of no along-span loads. With geometric updating, the effects of bowing on axial stiffness are incorporated, and the element can be used as a brace with post-buckling behavior included. The extra DOF associated with the interior nodes can be condensed out so that the number of global DOF does not increase. This process is described by (Hall and Challa 1995) where an example of a 2-segment element with a single interior node at mid-span acting as a brace is described. This multi-segment approach can also be used to model curved members approximately. Treatment of multi-segment elements with interior nodes is also provided in the companion paper for the elastofiber element.

CONCLUSIONS

A procedure for efficient three-dimensional nonlinear time-history analysis of steel-framed buildings is derived. In this method, four types of elements are employed: panel zone, plastic hinge

beam, elastofiber beam, and diaphragm. The panel zone element is intended to model the three-dimensional nonlinear shear behavior of joints in steel moment frame buildings while the plastic hinge and elastofiber elements model the three-dimensional nonlinear axial and flexural behavior of beams and column. The diaphragm element is a 4-node elastic plane-stress element which models diaphragm action of the floors and roofs of buildings. In this paper, the overall setup of the structural model, the analysis procedure, and the theory for the panel zone element and the plastic hinge beam element are described. Nonlinear panel zone shear and beam plastic hinging are included. Through geometric updating, the method allows large nodal translations and rotations so as to be able to follow the response of a building into the collapse regime. The theory for the elastofiber beam element along with illustrative examples are given in a companion paper.

References

Allahabadi, R. and G. H. Powell (1988). DRAIN-2DX user guide. Technical Report UCB/EERC-88-06, Earthquake Engineering Research Center, University of California, Berkeley, California.

Bertero, V. V., E. P. Popov, and H. Krawinkler (1972). Beam-column subassemblages under repeated loading. *Journal of the Structural Division, ASCE 98*(ST5), 1137–1159.

Carlson, A. (1999). Three-dimensional nonlinear inelastic analysis of steel moment-frame buildings damaged by earthquake excitations. Technical Report EERL 99-02, Earthquake Engineering Research Laboratory, California Institute of Technology, Pasadena, California.

Challa, V. R. M. (1992). Nonlinear seismic behavior of steel planar moment-resisting frames. Technical Report EERL 92-01, Earthquake Engineering Research Laboratory, California Institute of Technology, Pasadena, California.

Chopra, A. K. (1995). *Dynamics of Structures - Theory and Applications to Earthquake Engineering*. Prentice Hall.

Cook, R. D., D. S. Malkus, and M. E. Plesha (1989). *Concepts and Applications of Finite Element Analysis (Third Edition)*. John Wiley and Sons, New York.

El-Tawil, S. and G. G. Deierlein (1996). Inelastic dynamic analysis of mixed steel-concrete space frames. Technical Report Structural Engineering 96-05, Cornell University, Ithaca, New York.

Fielding, D. J. and W. F. Chen (1973). Steel frame analysis and connection shear deformation. *Journal of the Structural Division, ASCE 99*(ST1), 1–18.

Filippou, F. and M. L. Romero (1998). Nonlinear and dynamic analysis from research to practice. In N. K. Srivatsava (Ed.), *Structural Engineering World Wide 1998*, pp. T101–3. Elsevier Science Ltd., New York.

Hall, J. F. (1995). Parameter study of the response of moment-resisting steel frame buildings to

near-source ground motions. Technical Report EERL 95-08, Earthquake Engineering Research Laboratory, California Institute of Technology, Pasadena, California.

Hall, J. F. and V. R. M. Challa (1995). Beam-column modeling. *Journal of Engineering Mechanics 121*(12), 1284–1291.

Kassimali, A. (1983). Large deformation analysis of elastic-plastic frames. *Journal of the Structural Division, ASCE 109*(8), 1869–1886.

Kato, B. (1982). Beam-to-column connection research in japan. *Journal of the Structural Division, ASCE 108*(ST2), 343–360.

Krawinkler, H., V. V. Bertero, and E. P. Popov (1975). Shear behavior of steel frame joints. *Journal of the Structural Division, ASCE 101*(ST11), 2317–2336.

Krawinkler, H. and E. P. Popov (1982). Shear behavior of moment connections and joints. *Journal of the Structural Division, ASCE 108*(ST2), 373–391.

Krishnan, S. (2003). Three-dimensional nonlinear analysis of tall irregular steel buildings subject to strong ground motion. Technical Report EERL 2003-01, Earthquake Engineering Research Laboratory, California Institute of Technology, Pasadena, California.

Kunnath, S. K. (1995). Enhancements to program IDARC: Modeling inelastic behavior of welded connections in steel moment-resisting frames. Technical Report NIST GCR 95-673, Building and Fire Research Laboratory, National Institute of Standards and Technology, Gaithersburg, Maryland.

Kunnath, S. K., A. M. Reinhorn, and R. Lobo (1992). IDARC Version 3.0: A program for the inelastic damage analysis of reinforced concrete structures. Technical Report NCEER-92-0022, National Center for Earthquake Engineering Research, University at Buffalo, State University of New York, Buffalo, New York.

Lobo, R. (1994). IDARC3D: Inelastic damage analysis of reinforced concrete structures in three dimensions. Technical report, National Center for Earthquake Engineering Research, University at Buffalo, State University of New York, Buffalo, New York.

Lobo, R. F., M. J. Skokan, S. C. Huang, and G. C. Hart (1998). Three-dimensional analysis of a 13-story steel building with weld connection damage. In N. K. Srivatsava (Ed.), *Structural Engineering World Wide 1998*, pp. T114–2. Elsevier Science Ltd., New York.

Mazzoni, S., F. McKenna, and G. L. Fenves (2005). Opensees command language manual. Technical Report http://opensees.berkeley.edu/, Pacific Earthquake Engineering Research (PEER).

Oran, C. (1973a). Tangent stiffness in plane frames. *Journal of the Structural Division, ASCE 99*(6), 973–985.

Oran, C. (1973b). Tangent stiffness in space frames. *Journal of the Structural Division, ASCE 99*(6), 987–1001.

Park, Y. J., A. M. Reinhorn, and S. K. Kunnath (1987). IDARC: Inelastic damage analysis of reinforced concrete frame-shearwall structures. Technical Report NCEER-87-0008, National Center for Earthquake Engineering Research, State University of New York at Buffalo.

Pinkney, R. B. (1973). Cyclic plastic analysis of structural steel joints. Technical Report UCB/EERC-73-15, Earthquake Engineering Research Center, University of California, Berkeley, California.

Popov, E. P. and H. Petersson (1978). Cyclic metal plasticity: Experiments and theory. *Journal of the Engineering Mechanics Division, ASCE 104*(EM6), 1371–1388.

Powell, G. H. and S. Campbell (1994). DRAIN-3DX element description and user guide for element type01, type05, type08, type09, type15, and type17. Technical Report UCB/SEMM-94/08, Structural Engineering Mechanics and Materials, University of California, Berkeley, California.

Prakash, V., G. H. Powell, and S. Campbell (1994). DRAIN-3DX base program description and user guide, Version 1.10. Technical Report UCB/SEMM-94/07, Structural Engineering Mechanics and Materials, University of California, Berkeley, California.

Przemeniecki, J. (1968). *Theory of Matrix Structural Analysis*. McGraw-Hill Book Co., New York, NY.

Salmon, C. G. and J. E. Johnson (1980). *Steel Structures - Design and Behavior*. Second Edition. Harper & Row, Publishers, New York, NY.

Table 1: Tangent Coefficients, a_T, b_T, and c_T

Active Plastic Hinges	a_T	b_T	c_T
None	a	b	c
Node 1 only	$a\frac{k_1}{k_1+a}$	$b\frac{k_1}{k_1+a}$	$c-\frac{b^2}{k_1+a}$
Node 2 only	$a-\frac{b^2}{k_2+c}$	$b\frac{k_2}{k_2+c}$	$c\frac{k_2}{k_2+c}$
Nodes 1 and 2	$\frac{k_1\left[a(k_2+c)-b^2\right]}{(k_1+a)(k_2+c)-b^2}$	$\frac{bk_1k_2}{(k_1+a)(k_2+c)-b^2}$	$\frac{k_2\left[c(k_1+a)-b^2\right]}{(k_1+a)(k_2+c)-b^2}$

Table 2: Nine Plastic Hinge Cases Used for Determining $\left\{R_{ph}^{'l+1}\right\}_L$

Case	**Plastic Hinges**	M_1^{l+1}	M_2^{l+1}	κ_1^{l+1}	κ_2^{l+1}
1	None	$\mid * \mid < M_p^{l+1}$	$\mid * \mid < M_p^{l+1}$	$= \kappa_1^l$	$= \kappa_2^l$
2	Node 1	$= M_p^{l+1}$	$\mid * \mid < M_p^{l+1}$	$> \kappa_1^l$	$= \kappa_2^l$
3	Node 1	$= -M_p^{l+1}$	$\mid * \mid < M_p^{l+1}$	$< \kappa_1^l$	$= \kappa_2^l$
4	Node 2	$\mid * \mid < M_p^{l+1}$	$= M_p^{l+1}$	$= \kappa_1^l$	$> \kappa_2^l$
5	Node 2	$\mid * \mid < M_p^{l+1}$	$= -M_p^{l+1}$	$= \kappa_1^l$	$< \kappa_2^l$
6	Nodes 1 and 2	$= M_p^{l+1}$	$= M_p^{l+1}$	$> \kappa_1^l$	$> \kappa_2^l$
7	Nodes 1 and 2	$= M_p^{l+1}$	$= -M_p^{l+1}$	$> \kappa_1^l$	$< \kappa_2^l$
8	Nodes 1 and 2	$= -M_p^{l+1}$	$= M_p^{l+1}$	$< \kappa_1^l$	$> \kappa_2^l$
9	Nodes 1 and 2	$= -M_p^{l+1}$	$= -M_p^{l+1}$	$< \kappa_1^l$	$< \kappa_2^l$

List of Figure Captions

Figure 1. Element Arrangement in Frame Model, Showing Joint Nodes, Attachment Points, Local Beam Nodes, and Coordinate Systems.

Figure 2. Panel Zone Shear Caused by Beam and Column Moments at the Joint.

Figure 3. The Four Rotational Degrees of Freedom of a Panel Zone Element.

Figure 4. Joint Region of the Associated Column (Left) and Representation as a Panel Zone Element (Right).

Figure 5. Shear Stress-Strain Back Bone Curve for a Panel Zone Element.

Figure 6. Panels ① (Top) and ② (Bottom) Showing Dimensions and Degrees of Freedom (Left) and Edge Shear Forces (Right).

Figure 7. DOF of the Plastic Hinge Beam Element Showing Nodal Translations/Rotations and Nodal Forces/Moments.

Figure 8. Sign Convention for Internal Forces and Moments in a Plastic Hinge Beam Element.

Figure 9. $P - M_{pY'} - M_{pZ'}$ Interaction Diagrams Used for the Plastic Hinge Element.

Figure 10. Panel Zone Deformation Geometry for Construction of $[T_2]$ for a Column.

Figure 11. Panel Zone Deformation Geometry for Construction of $[T_2]$ for a Beam.

Figure 12. Panel Zone Deformation Geometry for Construction of $[T_2]$ for a Beam (Contd.).

Figure 13. $P - \epsilon$ Relation for Plastic Hinge Element.

Figure 14. Geometry of Plastic Hinge Beam Element for Bending and Shearing in the $X' - Z'$ Plane.

Figure 15. Effective Shear Areas for Wide-Flange and Box Sections.

Figure 16. $M^h - \kappa$ Relation at a Plastic Hinge.

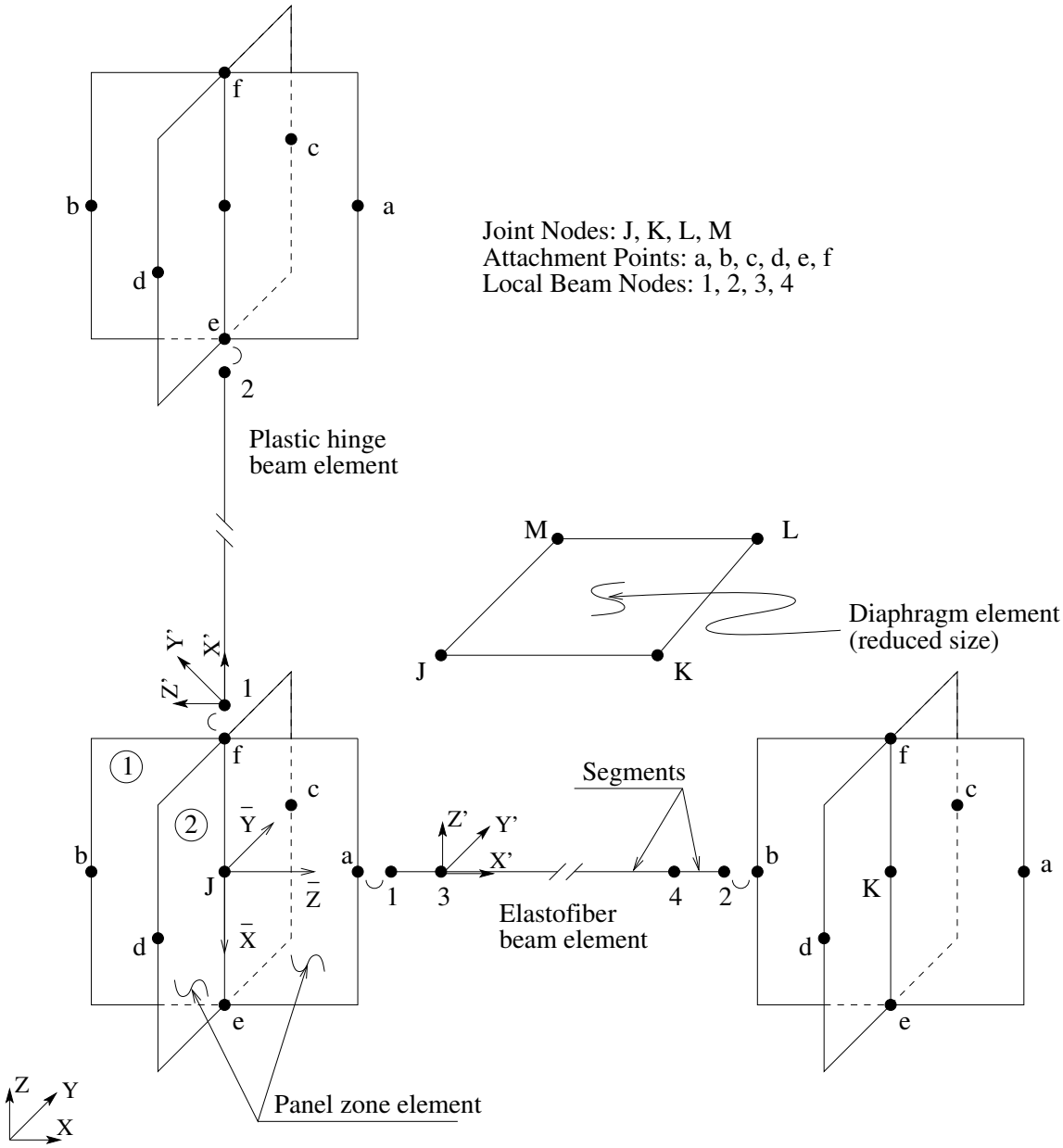

Figure 1: Element Arrangement in Frame Model, Showing Joint Nodes, Attachment Points, Local Beam Nodes and Coordinate Systems

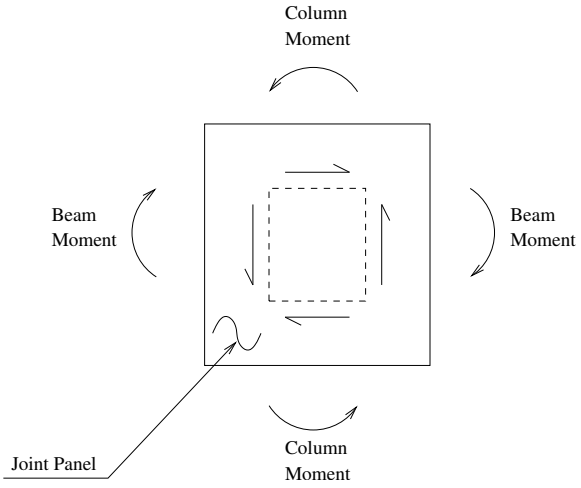

Figure 2: Panel Zone Shear Caused by Beam and Column Moments at the Joint

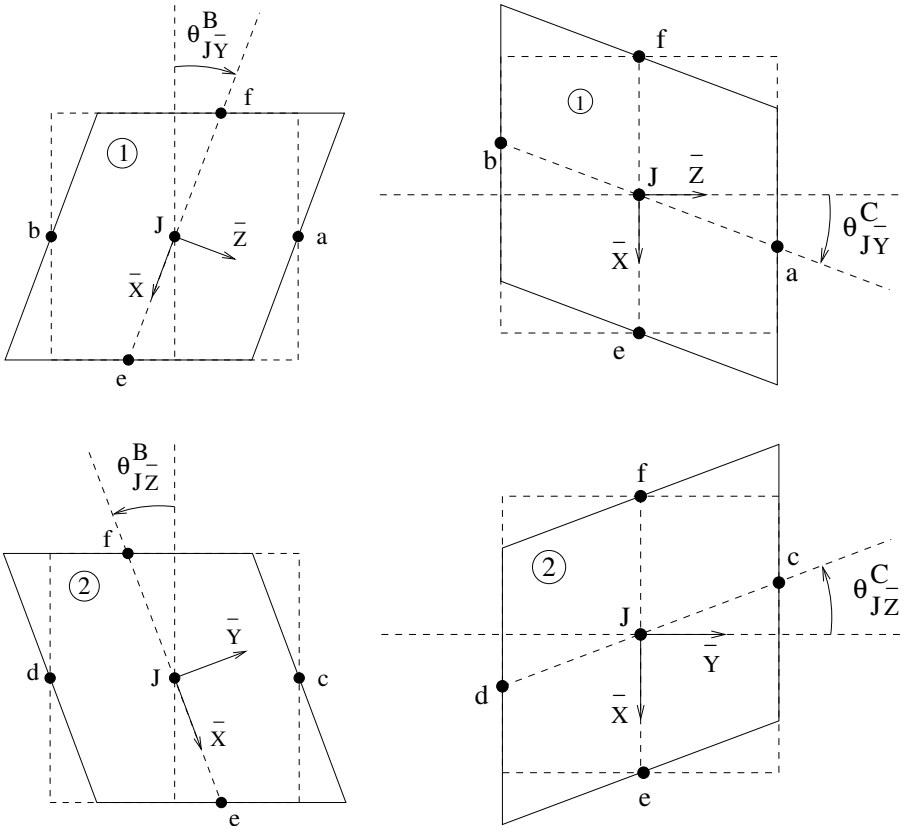

Figure 3: The Four Rotational Degrees of Freedom of a Panel Zone Element

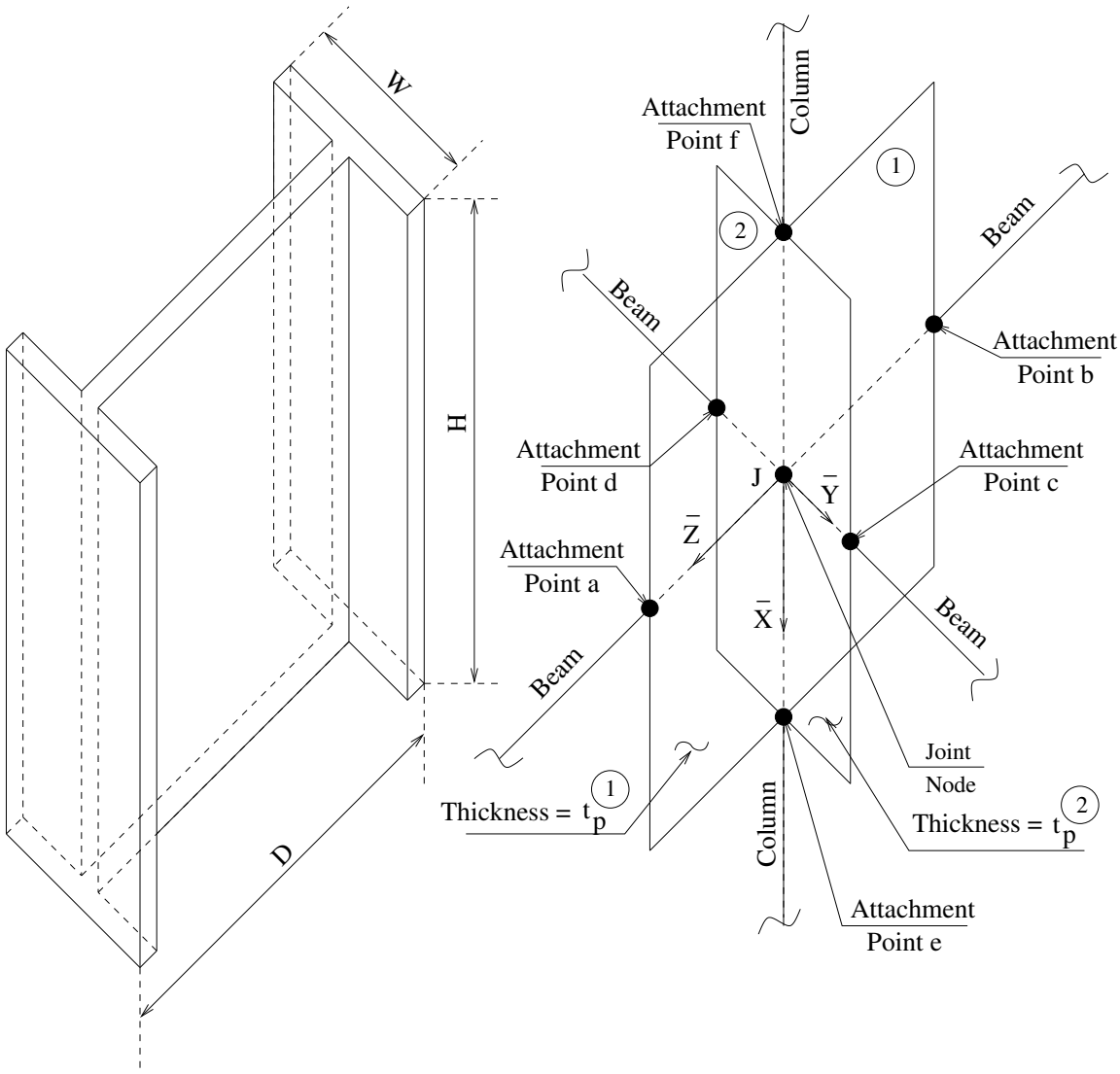

Figure 4: Joint Region of the Associated Column (Left) and Representation as a Panel Zone Element (Right)

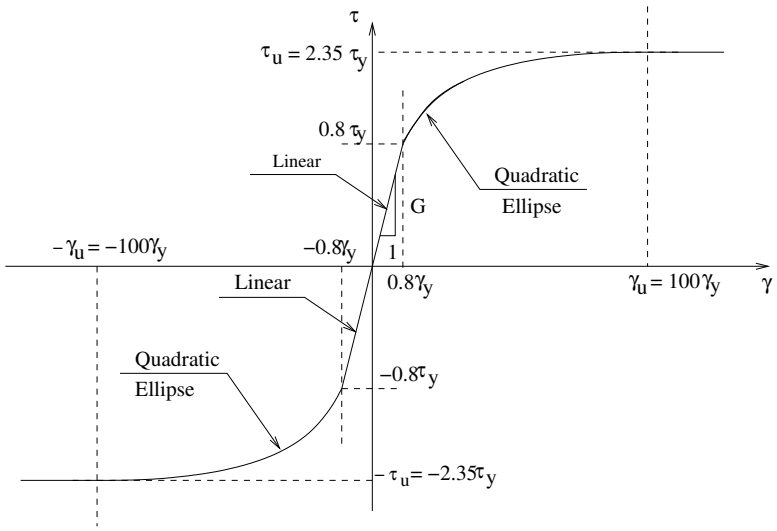

Figure 5: Shear Stress-Strain Back Bone Curve for a Panel Zone Element

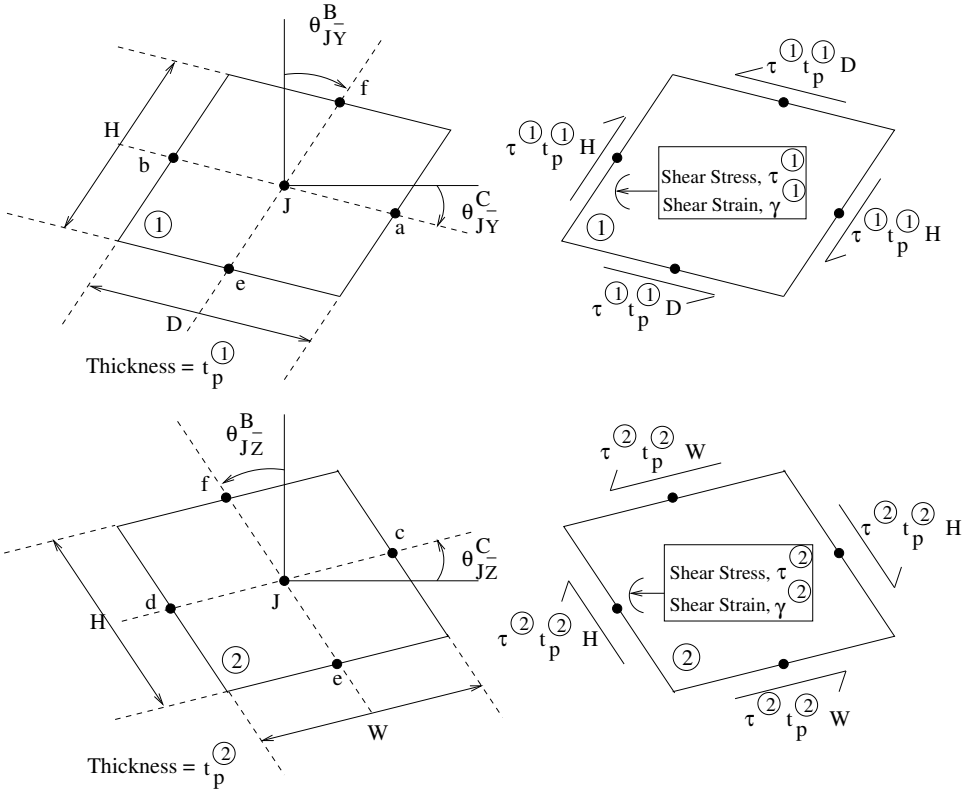

Figure 6: Panels ① (Top) and ② (Bottom) Showing Dimensions and Degrees of Freedom (Left) and Edge Shear Forces (Right)

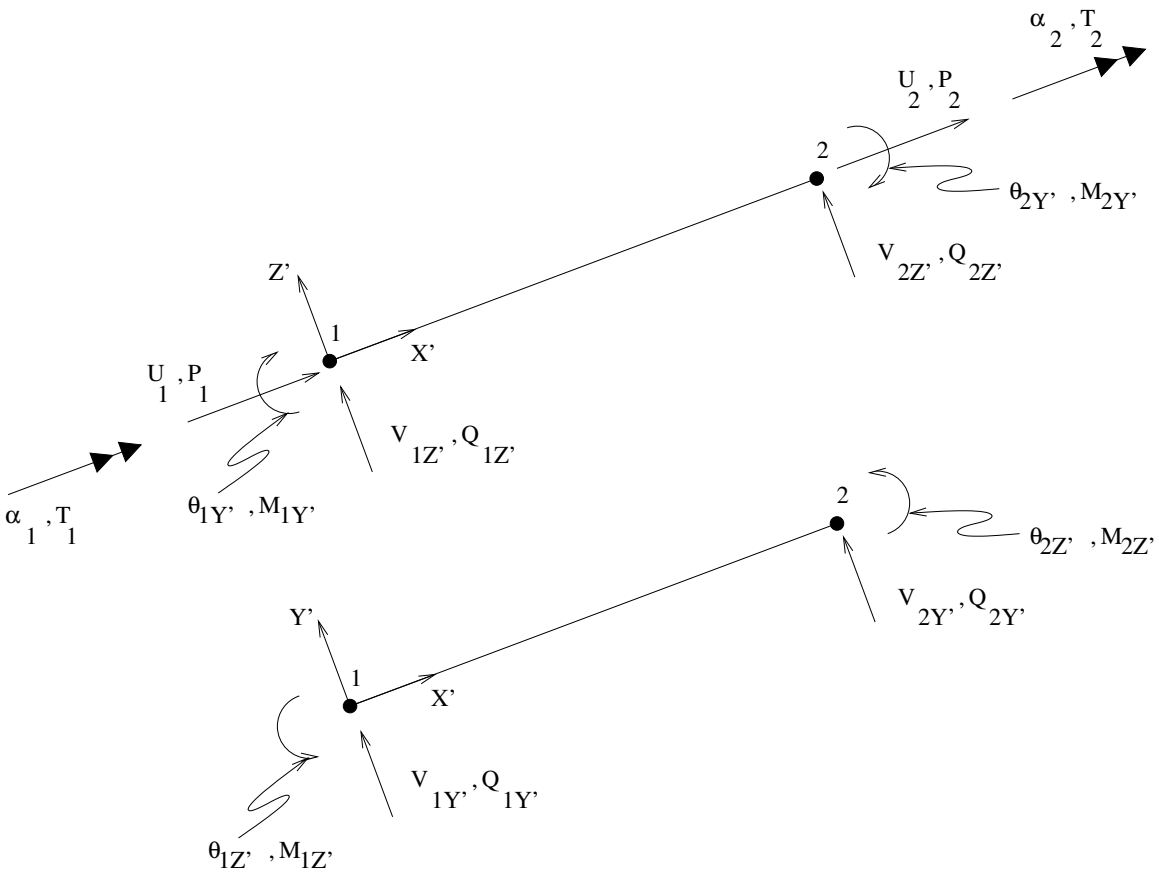

Figure 7: DOF of the Plastic Hinge Beam Element Showing Nodal Translations/Rotations and Nodal Forces/Moments

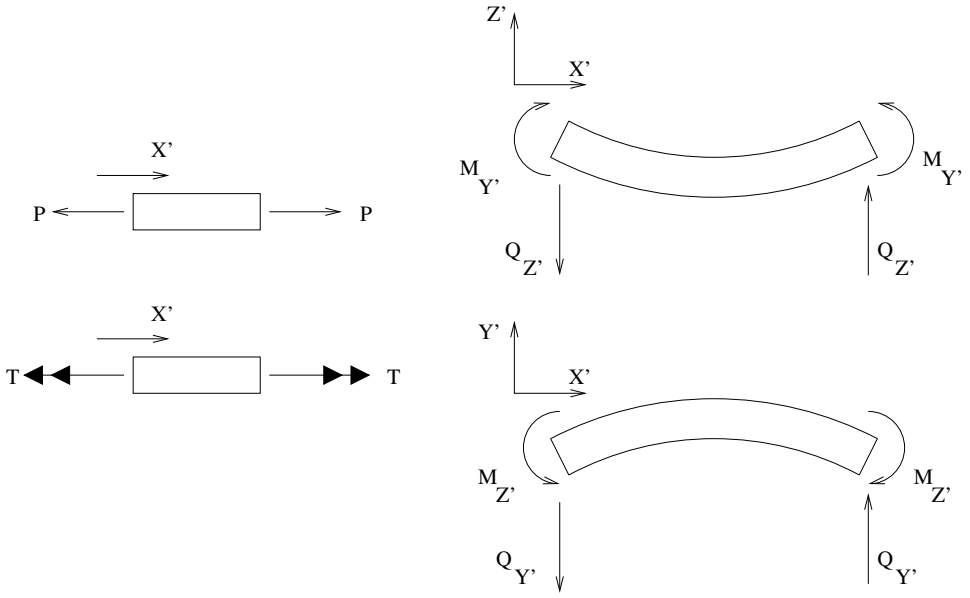

Figure 8: Sign Convention for Internal Forces and Moments in a Plastic Hinge Beam Element

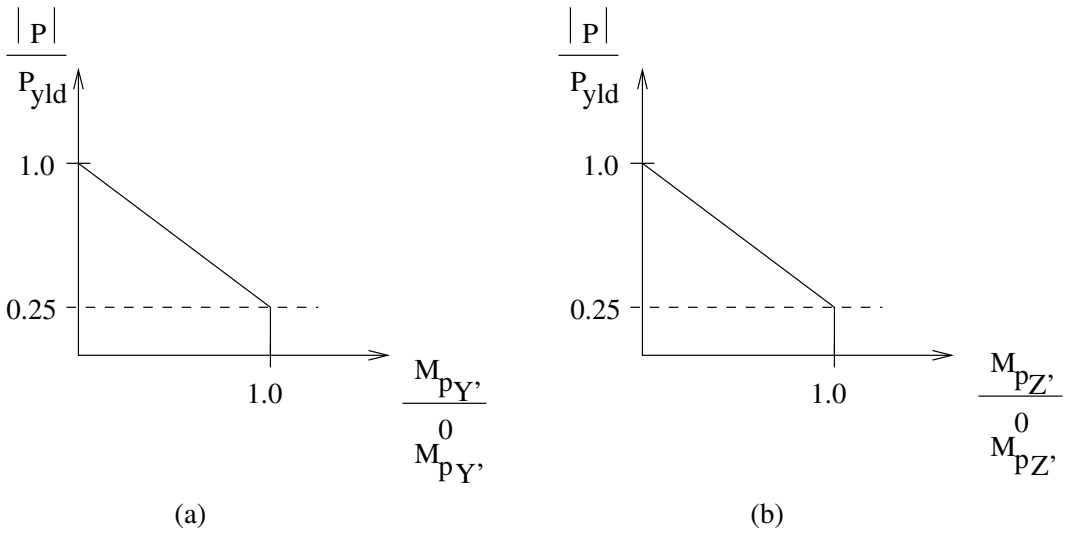

Figure 9: $P - M_{pY'} - M_{pZ'}$ Interaction Diagrams Used for the Plastic Hinge Element

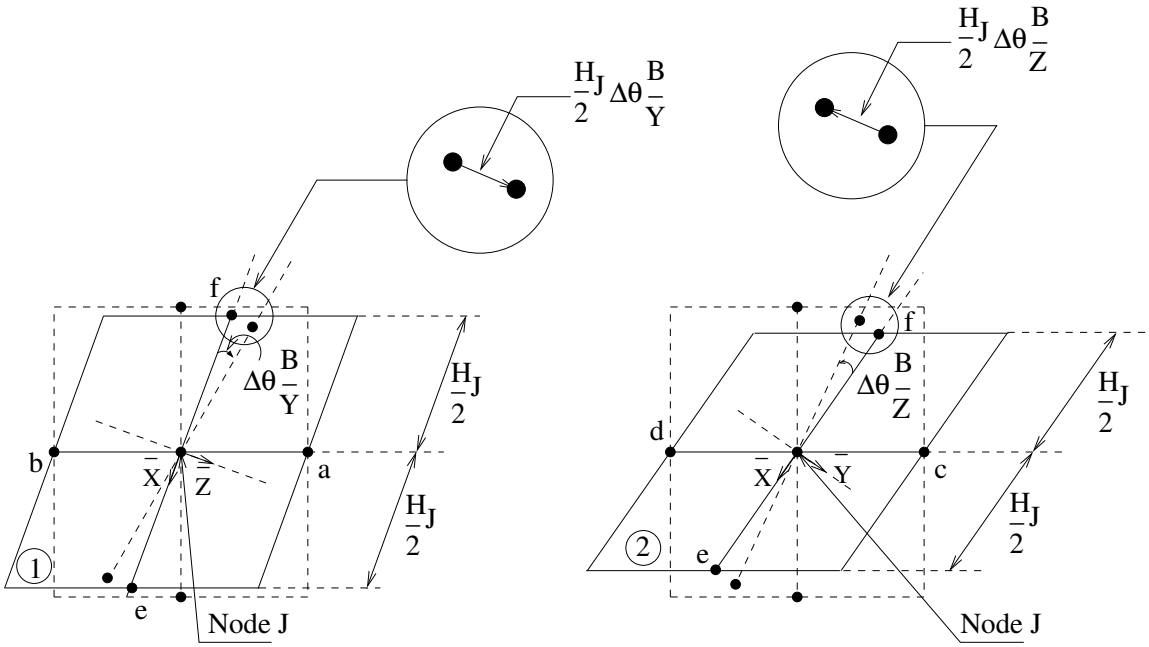

Figure 10: Panel Zone Deformation Geometry for Construction of $[T_2]$ for a Column

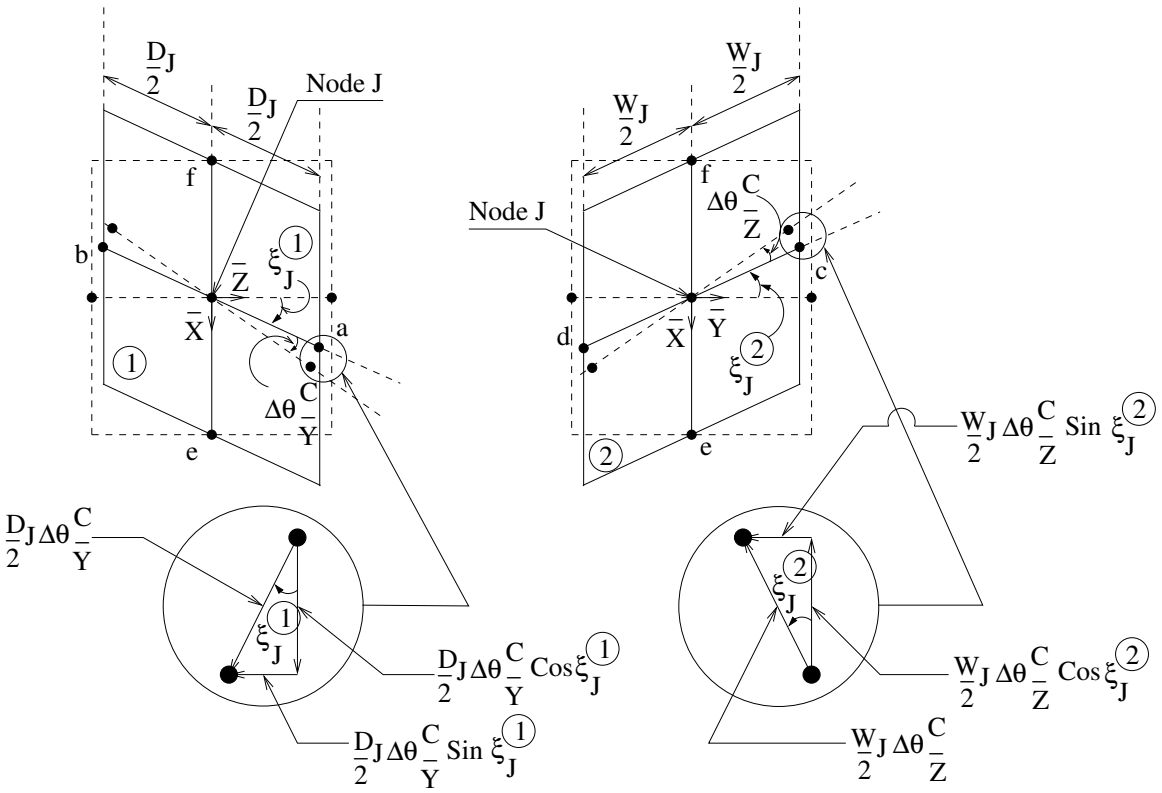

Figure 11: Panel Zone Deformation Geometry for Construction of $[T_2]$ for a Beam

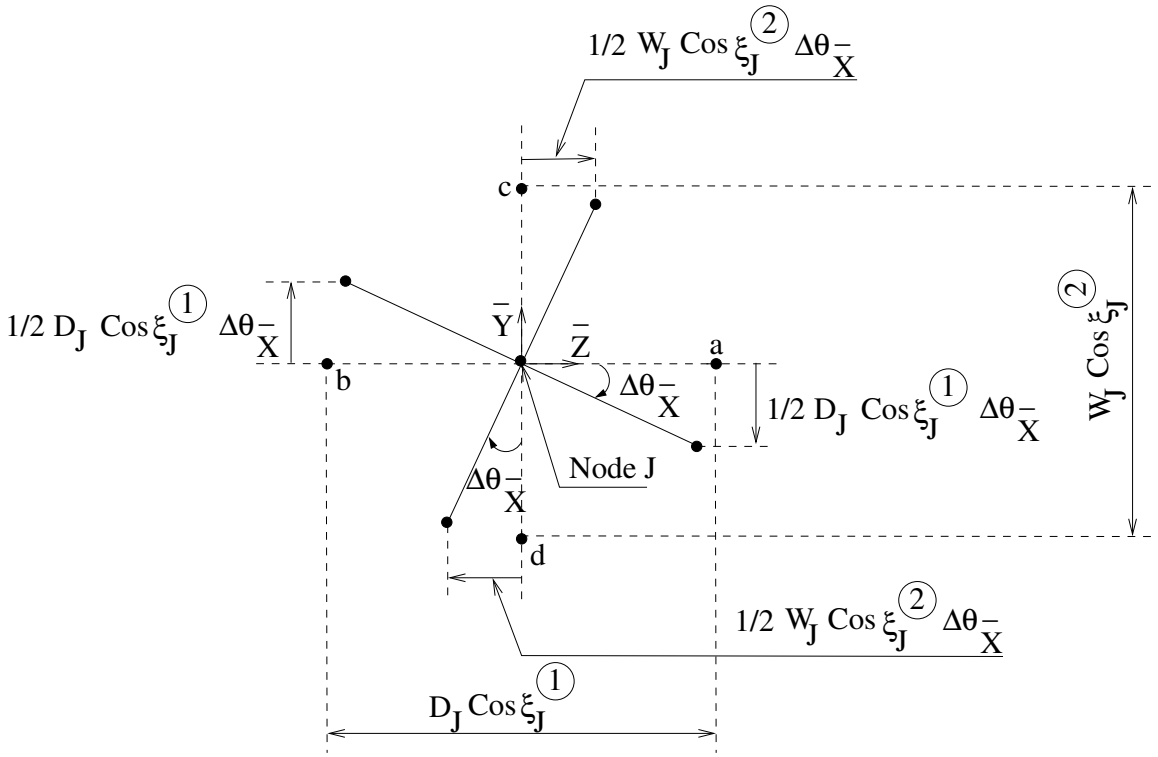

Figure 12: Panel Zone Deformation Geometry for Construction of $[T_2]$ for a Beam (Contd.)

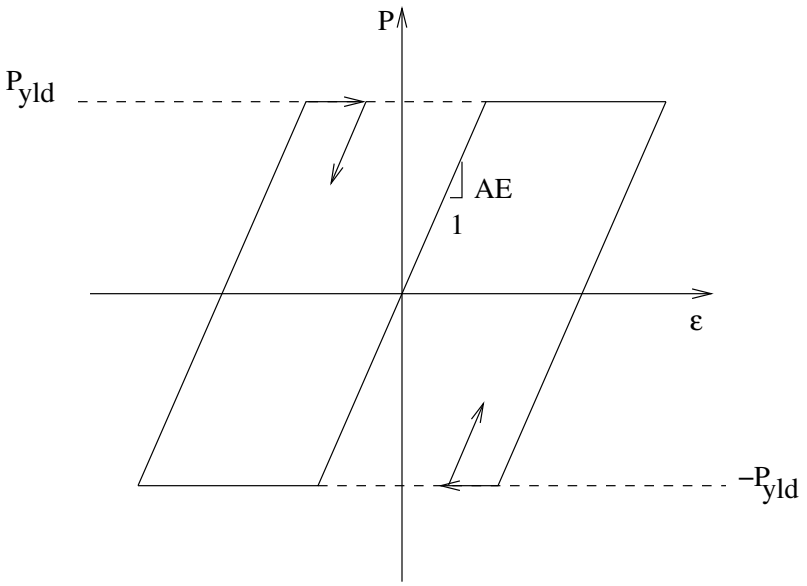

Figure 13: $P - \epsilon$ Relation for Plastic Hinge Element

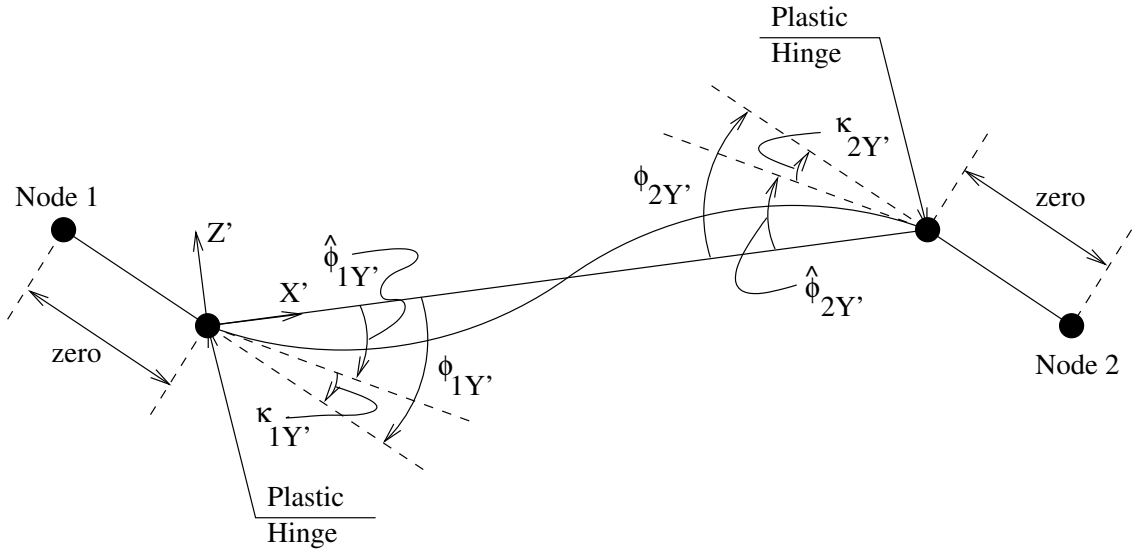

Figure 14: Geometry of Plastic Hinge Beam Element for Bending and Shearing in the $X' - Z'$ Plane

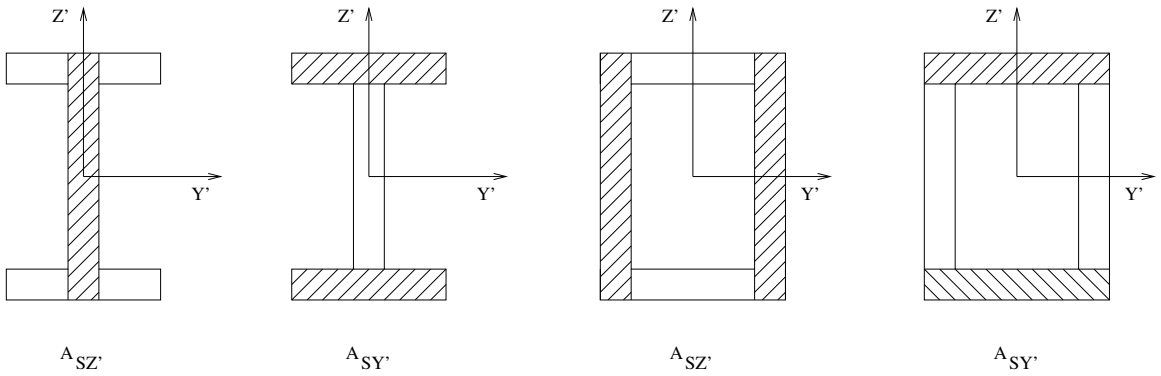

Figure 15: Effective Shear Areas for Wide-Flange and Box Sections

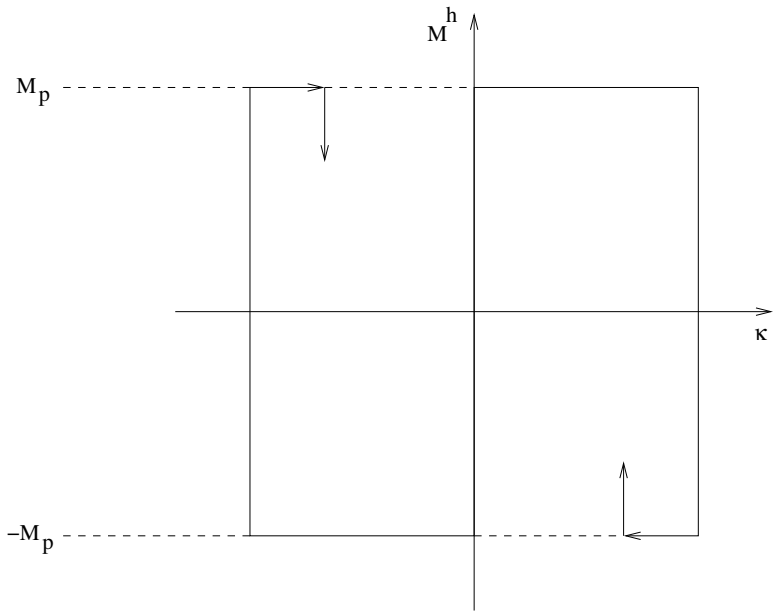

Figure 16: $M^h - \kappa$ Relation at a Plastic Hinge